Università degli Studi di Padova

Dipartimento di Ingegneria Industriale
Laurea Magistrale in Ingegneria Aerospaziale

Analysis and Optimization of a Subsonic Intake for Civil Aircrafts

Laureando:
Marco Tavoso

Relatore:
Prof. Ernesto Benini
Correlatore:
Andrea Dal Monte, Ph.D.

Anno accademico 2018/2019

To my family,
my girlfriend
and my friends.
Thank you.

Contents

Introduction

An intake is that part of an aircraft engine whose aim is to enter the air into the gas generator and the fan, and so allowing the generation of thrust.

Thrust is produced by a contribution of high mass flow ratio and low flow acceleration, which is given by the fan, and low mass flow ratio and high flow acceleration, by nozzle.
The main difference between rocket engine and aircraft engine is this: for the first, oxidant material is stored in tank inside the structure, so as to allow propulsion even in void, and limit performance decrease as a function of altitude; for the second one, the oxidant is mixed with the common air and is inspired by the intake.
This second solution fits better for long time journey at fixed altitude and fuel consumption logics: in fact, an intake allows the aircraft to reduce overall masses, reduces costs linked with oxidant material transportation and also increases its efficiency.

In years the technology evolves, transforming simpler propeller engine into more complex and high speed fitting turbojet engines, until its last and most efficient version, the turbofan.

Basic principle to understand thrust generation is linked with momentum conservation equation, with a direct or indirect approach:

For the first one, if flow is reaching a bounding surface of the intake, the momentum flux term $\int \rho v^2 dA$ corresponds to a force F in same direction, while pressure term $\int p dA$ returns another force in the opposite.

If the resultant force on the enclosed body is positive downstream, theorem stands that:

$$F = \int_B (p + \rho v^2) dA \qquad (1)$$

For the indirect approach, a force S is produced as a consequence of the difference of momentum on the aircraft among intake section and nozzle flow. In case of rocket engine, intake contribution is absent, and the whole thrust is produced by accelerating exhaust gases by a convergent-divergent nozzle.

Overall thrust is given by:

$$S \; = \; \dot{m}_{in} \frac{1+f}{1+B} c_{eq} \; + \; m_{in} \frac{B}{1+B} c_{ef} \; - \; \dot{m}_{in} v \tag{2}$$

in which f stands for fuel mixture ratio, B is the by-pass ratio (turbofan only), c_{eq} is equivalent exhaust velocity (in subsonic or adapted nozzle configuration is equal to the exhaust velocity) and v stands for flight speed (intake air speed at far-field).

It is clear that, according to engine configuration (turbofan, turbojet or rocket), there are terms that could neglect, from the most complete formulation of a turbofan to the simplest used for rocket engine: in this case, B and v are equal to 0, and now $\dot{m}_{in}(1+f) \; = \; \dot{m}_{out}$.

To better understand intake contribution, consider a simple duct which feeds the engine.
When the aircraft is taking off, mass flow increases as a consequence of speed increase and turbogas acceleration.
When speed reaches cruise condition, and so, for a subsonic civil aircraft, a Mach number of 0.84, the engine is no longer able to inspire the air at such high speed: also, pressure, as a consequence of high altitude (9000 - 100000 m), drops, and to allow thrust generation, it must be increased before compressor work starts.
So, an intake has to feed air to the engine at a proper pressure, density and speed, and its work is especially investigated during in-design flight condition, which is represented usually by cruise flight speed.

The simplest way to understand intake work is, firstly, to consider the air as a perfect gas, and so obeying to ideal gas law:

$$pV \; = \; nRT \tag{3}$$

in which p is the static pressure, V is gas volume, n the number of moles, $R = cp - cv$ is perfect gas constant and T the absolute temperature.
For system with outflow, it is better the form of:

$$p \; = \; \rho RT \tag{4}$$

The intake lets the air to be slowed down by isentropic compression before entering the turbogas group.

Total pressure is given by:

$$p_0 = p \left(1 + \frac{k-1}{2} M^2 \right)^{\frac{k}{k-1}} \tag{5}$$

and it is defined as the pressure flux reaches if it is completed stopped in a stagnation condition.
During isentropic compression, total pressure doesn't vary (in particular, it doesn't decrease), as a consequence of irreversible transformation as friction, heat or shocks.

Total pressure, and in general total quantities, are really important in turbojet (and turbofan) engines, because, by means of the slower speed the air has while going throughout the machine, static quantities are really close to total quantities (at Mach number lower than 0.3, differences in terms of density are lower than 5%), and so as long as performance is a requirement of the engine, pressure drop has to be limited ad much as possible.

In real physical world, friction is almost impossible to neglect, and so it is mandatory to evaluate the amount of losses.
In a duct, losses due to friction are modelled by function of Reynolds number (in next chapter the description), which represents the ratio between inertia and viscous forces.
In laminar fluxes ($Re < 2300$), coefficient of friction f is given by $f = \frac{64}{Re}$, instead of turbulent flows in which f is function of both Re and roughness, but the equation description goes beyond this thesis purpose.

An intake has to slow down, by isentropic process, the airflow, but how?
In subsonic flight ($M < 1$), gas dynamics teaches that, by evaluating area equation:

$$\frac{du}{u} = \frac{1}{M^2 - 1}\frac{dA}{A} \tag{6}$$

an area reduction leads to an increase of speed, and so to reduce it, area must increase before reaching the compressor.

Due to the fact that, at subsonic speed, quantities variations propagate upstream, if the turbogas forces a determined value of airflow, and all the compression is not possible to make only by the intake, a phenomenon like the ram-effect happens: airflow slows down before entering the intake, and this is possible by means of a divergent shape imposed to the stream function upstream.
This effect is always produced while pilot reduces air request by "slowing down" the engine, before the phase of landing.

In this thesis, as it will be clearer in next chapters, wind tunnel data available are the type of this situation, and it is important to understand this process in order to investigate better how an intake works, and what the main feature of an intake are.

In order to realize a diverging shape which is also suitable for external aerodynamic purposes (drag performance), the simplest method to employ is to extrude, by a revolution around main axis, an airfoil.
An airfoil is the most important aerodynamic shape, because it is capable of vary speed and pressure around it in the most efficient way, and so it is clear that its main purpose is the design of aircraft wings.
An airfoil works on airflow by the sum of two different parameters concerning its (lack of) symmetry: angle of attack (respect to local wind) and camber (curvature of middle line).

For intake geometries, an airfoil is selected putting outside its suction side, characterized by the increase of local airspeed, while pressure edge is put inside. So, the diverging geometry profile is created by the revolution of airfoil pressure side, while drag reduction is performed by the suction side.

The part of the intake created by an airfoil is called cowl, and, as a consequence, leading edge becomes now the cowl lip.

Throughout the years, many geometries were taken into consideration for the shape of the intake cowl, especially by the NACA (National Advisory Commettee for Aeronautics), who developed a series of airfoil using mathematics equations.
In particular, the 1-series was developed as suitable for intake geometry, especially because of the absence of a closed trailing edge, and so a complete separation of fluxes between two sides of the shape.

Intake performances that mainly interest this thesis project are drag efficiency and pressure recovery. Drag efficiency concern external surface of the intake, and so outer side of the airfoil shape; pressure recovery is the ratio between the maximum pressure reached at the end of compression work before entering the compressor, and total pressure.
In order to relate better pressure recovery to flight speed, it is better to refer to an average coefficient of pressure, so:

$$C_p = \frac{p - p_\infty}{q_\infty} \tag{7}$$

where q_∞ is dynamic pressure at far-field:

$$q_\infty = \frac{1}{2}\rho v_\infty^2 \tag{8}$$

So as to investigate the behaviour of an intake at different condition of flight (far-field Mach Number M_∞ and mass flow), and in order to understand the importance of cowl shape in overall intake performance, analytic calculus is not enough, because too many variables are involved, especially for what concerns boundary layer and, consequently, fluid detachment from airfoil surfaces.

Fortunately, technology gives engineers the opportunity to do complex calculus process by simulating physical situation with a discretization of the problem faced: continuum mechanics can be investigated in a grid domain, in which, in every cell, equations are solved: overall solution comes from the contribution of every cell results. Computational Fluid Dynamics (CDF) employs the method of Finite Volume Method so as to reach, after many iterations, the solution.

So, the purpose of this thesis is to develop a CFD model whose aim is, firstly, to be validated by real wind tunnel tests, but in the end it will have to become the source of a new geometry which improves the performances of pressure recovery and drag penetration.

In order, the work will be done by:

1. extracting an existing geometry of an intake that was tested in wind tunnel;
2. understanding what are the main characteristics of a flow entering an aircraft engine, in terms of fluid detachment and sonic transition;
3. converting a series of tabulated points in a cowl geometry, creating a mesh around the shape to be enclosed by the right boundary;
4. setting up the proper physical model, which respects wind tunnel condition of test;
5. validating the model by wind tunnel results;
6. creating a 1-dimension model which is able to produce similar results data to be compared to CFD's ones;
7. optimizing the geometry with the same CFD model.

First chapter of the thesis focuses the attention on the geometry and physics of the problem, pursuing the goal of a CFD model development; the next one is focused on results of CFD model, in comparison to 1-d gas dynamics evaluations. The last chapter contains the optimization process, so as to improve intake performance by changing, in a mathematical way, its shape.

Chapter 1

Validation

First aim of this thesis project is to build up a CFD model which is able to predict the behaviour of fluxes along the inner surfaces of a subsonic intake. This type of aerodynamic intake must vary its mass flux at different speed of flight: the consequent behaviour of the air around the cowl lip will influence the properties inside the intake.

The best way to learn this type of aerodynamic process is to look at wind tunnel test validation, and the CFD model that will be developed has to reproduce geometries and boundaries of those tests.

In 1996, NASA conducted a series of simulations by wind tunnel on three different cowl geometries: the goal of the test was to understand how the Mach number of the inlet boundary influences fluid detachment and sonic transition at different mass flow ration of the engines.

NASA used three NACA 1-series cowl airfoils, with different cowl length and inner edges geometry.

The complete report used as reference and as a guide is *"A Complete Investigation of Three NACA 1-Series Inlets at Mach Numbers up to 0.92" by Richard J. Re and William K. Abeyounis of Langley Research Center, Hampton, Virginia.*

A brief table illustrates what kind of test were conducted, see in Appendix.

1.1 Geometry

For the purpose of this thesis, it was decided to investigate only one of the three cowl geometry available, because only one of those best fits the nacelle form which will be used in next chapters.

In fact, the geometry of cowl lip influences how air fluxes increase their speed while entering the intake: a small cowl lip best fits high subsonic speed, because it minimizes the speed increase, which results in less possibility of sonic transition; on the other hand, a bigger cowl lip could get low speed fluxes to follow better the geometry of the inner side of intake without detaching the boundary layer. So, only one of the three cowl geometry was a sufficient compromise to investigate a full aircraft intake at different flight speed: the NACA 1-85-100 with internal contraction ratio of 1.250. For a better explanation: 85 stands for the ratio between highlight cowl diameter and maximum cowl diameter, which is 85 %; 100 stand for ration between

cowl maximum diameter and cowl length, which is 100%.
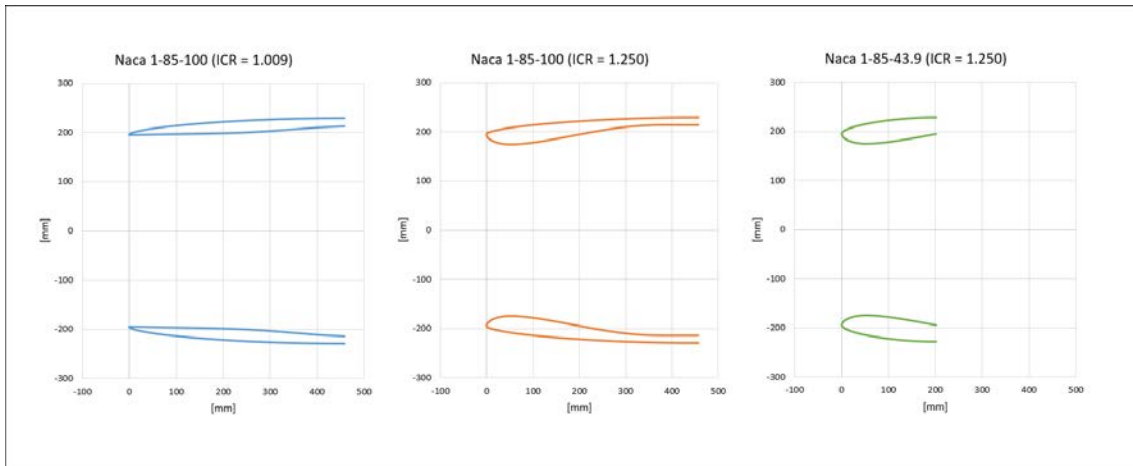In Figure 1 the comparison between the three cowl geometries.

Figure 1.1: Comparison of the three geometry of cowl airfoil presented in the reference text

Also, the second intake of Figure 1.1 (the choice) has the highest ratio between highlight diameter and inner cowl diameter, and so the maximum pressure recovery with this type of intake.
A question could be natural: why are these intakes so short? In fact, an actual civil aircraft has highlight diameter of its turbofan engines of about 1 meter or more, and these intakes have a dimensions less than an half of the current dimensions. This choice was of similitude: wind tunnel utilized in these tests worked at atmospheric temperature and pressure (sea level), and so, in order to simulate at same Reynolds number of a real engine working at 10 000 m, the simplest way was to reduce the diameter, and so the length, of the intakes.
So, the cowl geometry of the intake that will be studied is 457.2 mm long and its highlight diameter is of 390.27 mm.
In Figure 1.3, the CAD geometry of the intake extruded by a revolution around engine main axis

1.2   CFD Model

1.2.1   Law of the wall

Before setting up a computational grid for the physical model, the law of the wall for this particular problem has to be understood. In fact, when viscosity is present in a CFD model, a scale factor is introduced in the simulation: this factor separate the solution for flow field next to the airfoil from the one of flow at far-field, and so a procedure like scaling a mesh it's not so simple as in inviscid simulation. In fact, the parameter that explains the ratio between inertia forces and friction ones is the Reynold number: this non-dimensional quantity shows how much viscosity is important in the physics of the problem, and it depends on dimensional quantities like a reference length (a diameter or a chord length) and air speed:
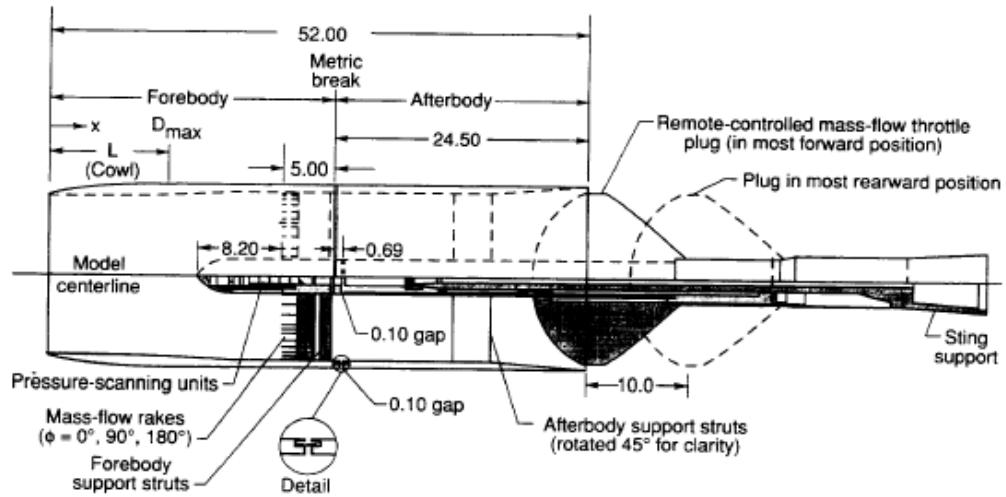
Figure 1.2: Simplified cross-sectional sketch of complete model. Linear dimensions are in inches.
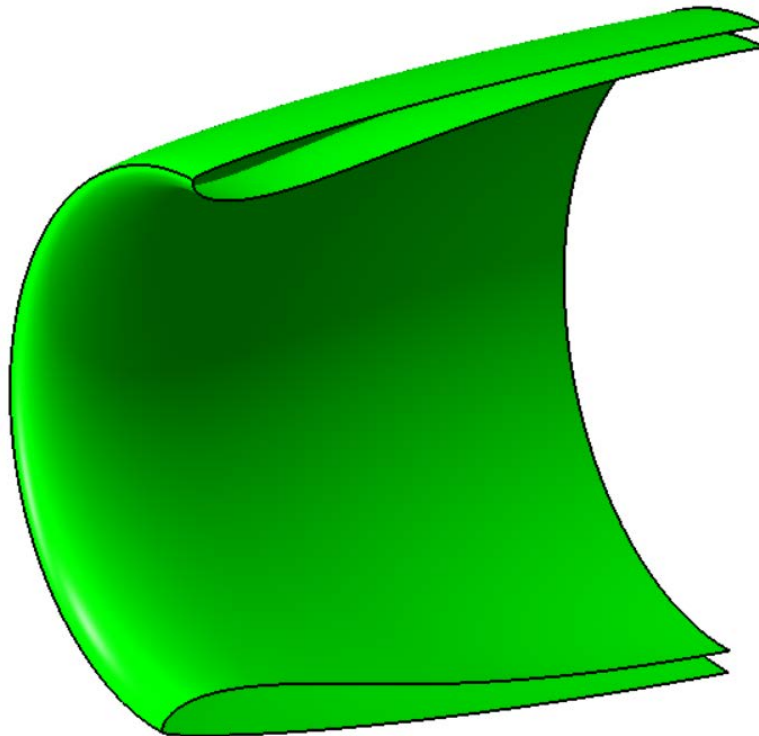
Figure 1.3: CAD geometry of the intake

$$Re = \frac{\rho_\infty * U_\infty * L}{\mu} \tag{1.1}$$

Also, Reynolds number marks the transition between laminar and turbulent flows. In particular, the turbulence is a phenomenon that, for computational reasons, has to be approximated by several mathematical models, in this case RANS (= Reynolds Averaged Navier-Stokes).

For this kind of simulation, in which a positive pressure gradient is present around the airfoil (pressure side especially), the most suitable RANS turbulence closure model to be set is $k - \omega\ SST$. This model is a combination of $k - \omega$, perfect choice around the airfoil, and $k - \epsilon$ far from wall. $k - \omega\ SST$ needs y+ value lower than 1. But what is y+?

In turbulence approximation, many non-dimensional quantities are used. In particular, $u+$ and $y+$ are called, respectively, dimensionless velocity and dimensionless wall distance. Values are as follows:

$$u+ = \frac{U}{u^*} \tag{1.2}$$

$$y+ = \frac{u^* \Delta s}{\nu} \tag{1.3}$$

where U is local velocity,

$$\nu = \frac{\mu}{\rho} \tag{1.4}$$

is kinematic viscosity, Δs is wall spacing and

$$u^* = \sqrt{\frac{\tau_{wall}}{\rho}} \tag{1.5}$$

is friction velocity.

Friction velocity is the results of dimensional analysis, and so is dependent from how friction is computed. In *Frank M. White's Fluid Mechanics 7th edition*, it is explained that, for a flat panel, friction coefficients are given by:

$$C_f = \frac{0.027}{Re_x^{1/7}} \tag{1.6}$$

$$\tau_{wall} = \frac{1}{2}\rho C_f U_\infty^2 \tag{1.7}$$

So, as a consequence of these parameters, it is possible to calculate the wall spacing needed by the first cell of a boundary layer extrusion (in meshing process) by knowing a y+ value. Because y+ marks the separation of viscous boundary layer and logarithmic boundary layer, its value is of fundamental importance for a RANS model. For $k - \omega\ SST$, as previously said, $y+ < 1$.

The employed theory is suitable for flat panels, not for airfoil, nevertheless, by some iteration, it is possible to set up the most correct value. Calculations give the value of y+ = 0.0014 mm, and so minimum wall spacing for the first cell will be set to 0.001 mm.

Mesh will be created by using Pointwise.
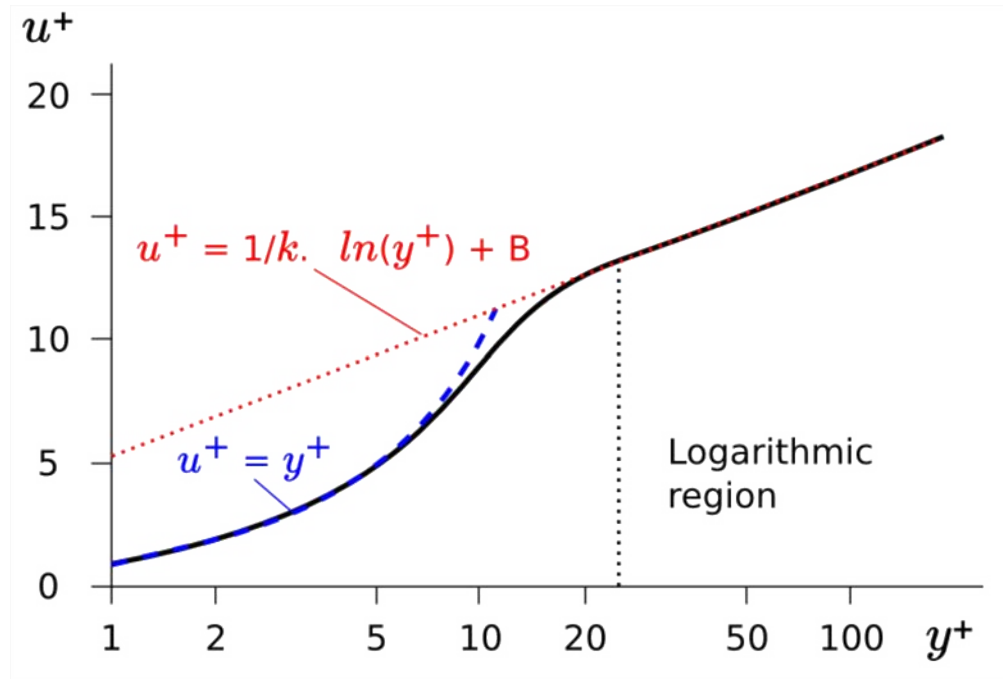
Figure 1.4: Law of Wall quantities

1.2.2   Mesh

For computational reasons, simulations will be conducted only with 2D axisymmetric model, and so validation will be possible only for 0 angle of attack.
This way was pursued in order to minimize the number of cells (used for discretization grid) in the mesh, and so the overall computational time: a 3D model, needed while investigating the intake at non-zero angle of attack, could lead this number easily over 1 million, instead of maximum 100 thousands cells of the choice.
Many types of mesh were taken into consideration, but, so as to better simulate sonic transitions (which are impossible to prevent at high Mach number), it was decided to use a C-grid structured mesh.
A C-grid mesh allows a structured mesh, which is more suitable for the kind of flux it will be simulated, to cover perfectly the geometry of an airfoil with an open trailing edge shape, like the one of the cowl.

First of all, once the airfoil geometry is loaded, curves has to be converted in connector, functions of Pointwise which will indicate domain boundaries. Extensions were added after trailing edge so as to prevent solution fluctuations, caused by throat section, to reach mass flow inlet section.
A connector is divided into several control points, which stand for curve sizing: the distribution of cells on airfoil "surface" was set from 0.01 mm at the leading edge to 1 mm at the outlet (aspect ratio inside boundary layer could be higher than other cells').
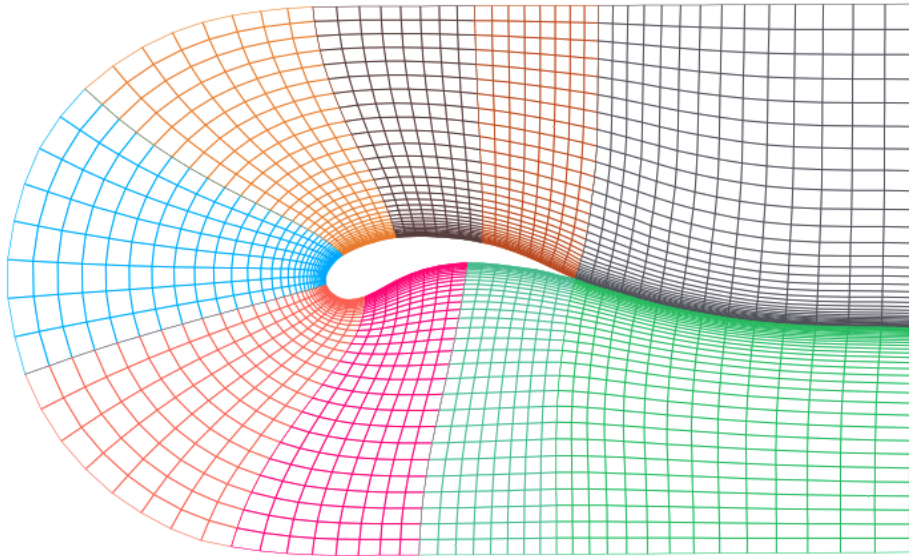
Figure 1.5: C-grid mesh example
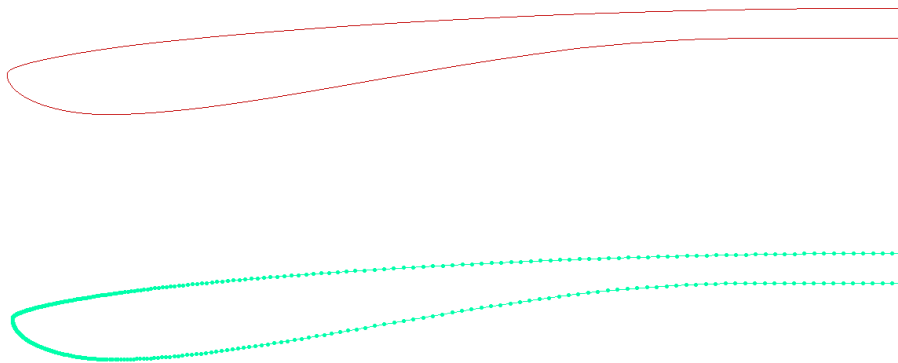
Figure 1.6: Database airfoil (up)converted to a connector, with the proper size (down)

Once a connector is sized properly, it's time to extrude boundary layer. Pointwise makes available different extrusion strategies in order to best generate the prism layer around an airfoil: this time, an algebraic extruder seems to be the best choice, because first cell height and the dimension of each step could be controlled accurately. As said previously, first cell height is set to 0.001 mm. At the trailing edge, boundary constraints in y direction force the extrusion to follow the y-axis.

So, a complete boundary layer, composed by 50 layers, results, in the outermost edge, composed by perfect square cells at leading edge and by high-aspect-ratio cells at trailing edge.

The last layer will be the starting point for the domain main mesh.
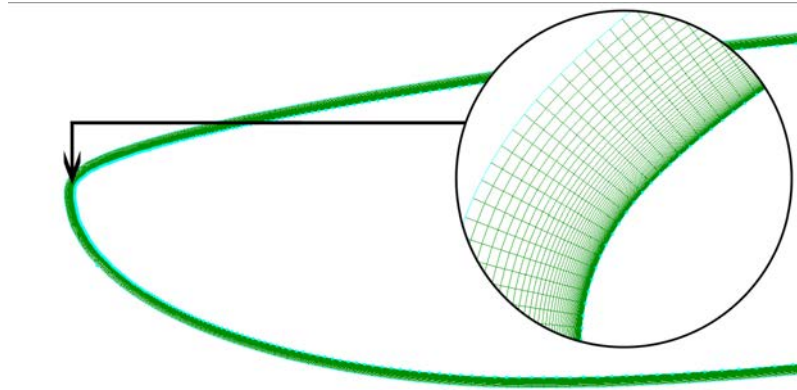
Figure 1.7: Boundary layer detail, at leading edge
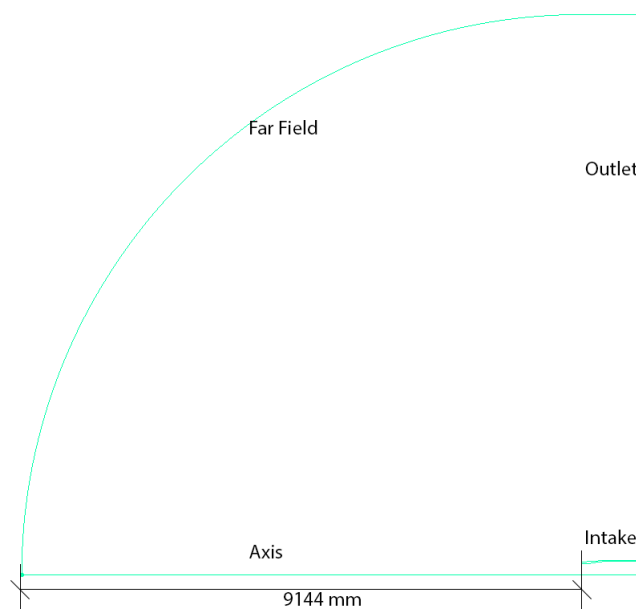
Figure 1.8: Domain dimension of the CFD model

After that, boundary domain dimension has to be selected in order to minimize the aerodynamic influence on the intake: far field was placed at 20 cowl-length ($457.2 * 20 = 9144$ mm) from cowl lip, in an arc geometry (Figure 1.8 as reference).

So as to generate a structured mesh, the main grid has to be divided in n sub-block, each of them with its own boundary, closed at one side to the far-field (or axis) and at the other to the boundary layer of the airfoil. Every connector of each block must contain, at alternate edges, the same number of points.
Also, near leading edge, on inner side, is placed a point in which boundary layer and three blocks will converge: this is necessary in order to create a mesh as regular as possible.

When all the connector has the proper dimension, the grid could be generated.
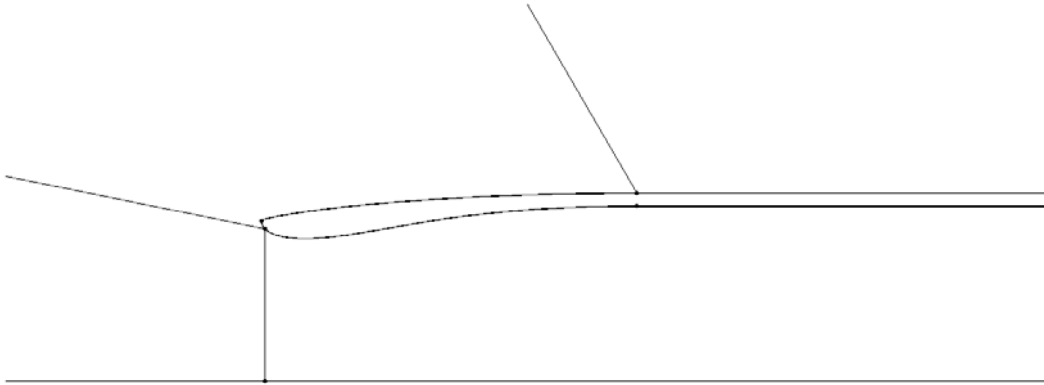
Figure 1.9: Block division, made up by several connectors starting from outer edges of boundary layer

The resultant mesh has a high level of skewness near leading edge, due to the fact that, here, sizing has the thinnest displacement. So as to improve mesh quality, Pointwise has developed an embedded function of grid optimization: the target of this process could be skewness equiangle, aspect ratio, area distribution and many others. The first is the most important parameter for mesh quality.
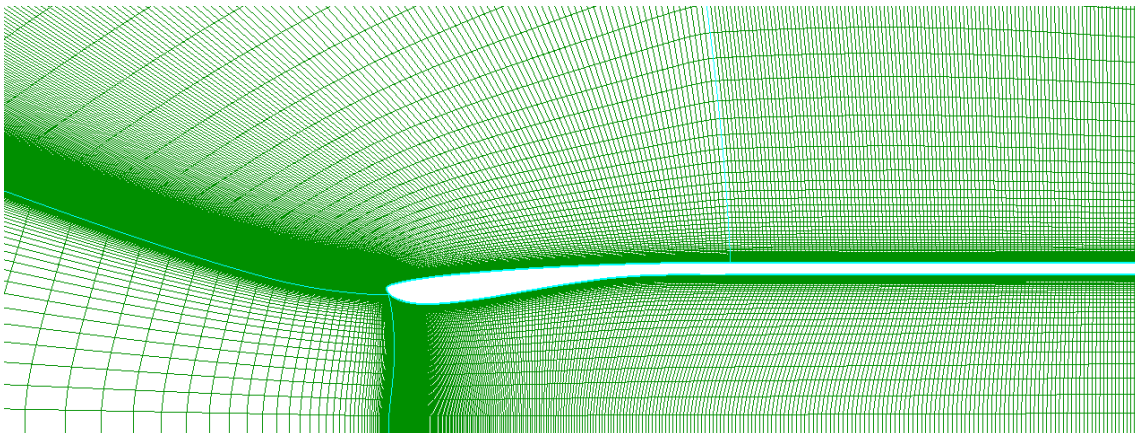
Figure 1.10: C-grid mesh growth from boundary layer to domain boundaries

After many iteration, the equiangle skewness reaches 0.60 (Ansys Fluent requests values lower than 0.95).
At the end, mesh dimension consists in 81 363 cells.

Boundary conditions are set to:
- Far Field: Pressure Far Field
- Outlet: Pressure Outlet
- Axis: Axis
- Nacelle (in and out): Wall
- Mass Flow: Mass Flow Inlet

Next part will be developed in Ansys Fluent.

1.2.3   Physical model

The physical model is developed in Ansys Fluent: operating condition has to be set equal to the environmental condition in which wind tunnel tests were conducted.
So, in boundary condition menu, pressure at far-field and outlet is set to 101325 Pa (1 atmosphere), and, in operating condition menu, is set to zero.
Also, temperature is set to 300 K (there isn't any sort of indication about the temperature of the test, so this is a hypothesis).
The model is set to 2D axis-symmetric, and it has to be scaled (Pointwise uses [mm] as unit length, Fluent is set to [m]).
Viscosity simulation is conducted by RANS model k-w SST, whose main requirement is $y+ < 1$ on every wall boundary condition (as it has already been explained in previous sections).

Energy equation is set to ON (it is a compressible flow simulation) and gas properties has to be varied:
- Density: Ideal Gas
- Cp (Specific Heat): Constant (1006.43 J/kg*K) [default]
- Thermal Conductivity: Constant (0.0242 W/m*K) [default]
- Viscosity: Sutherland (C1 = 1.716e-05; C2 = 273.11) [kg/m*s]
- Molecular Weight: Constant (29.966 kg/kgmol) [default]

The main conditions to be set are Mach number at far field and mass flow at mass flow inlet: these quantities will be entered in the software according to the values indicated in wind tunnel test.

For a preliminary setting of the model, Mach = 0.84 and Mass Flow = 20 kg/s are put as boundary condition. The goal, now, is to find the best calculus model between Density Based and Pressure Based.

According to Fluent's User Guide, *The density-based solver solves the governing equations of continuity, momentum, and (where appropriate) energy and species transport simultaneously (i.e., coupled together). Governing equations for additional*

scalars will be solved afterwards and sequentially [..]. Because the governing equations are non-linear (and coupled), several iterations of the solution loop must be performed before a converged solution is obtained."

Steps are:

1. *Update the fluid properties based on the current solution. (If the calculation has just begun, the fluid properties will be updated based on the initialized solution.)*
2. *Solve the continuity, momentum, and (where appropriate) energy and species equations simultaneously.*
3. *Where appropriate, solve equations for scalars such as turbulence and radiation using the previously updated values of the other variables.*
4. *When interphase coupling is to be included, update the source terms in the appropriate continuous phase equations with a discrete phase trajectory calculation.*
5. *Check for convergence of the equation set.*

The two main formulation are:

- *implicit: For a given variable, the unknown value in each cell is computed using a relation that includes both existing and unknown values from neighboring cells. Therefore each unknown will appear in more than one equation in the system, and these equations must be solved simultaneously to give the unknown quantities.*
- *explicit: For a given variable, the unknown value in each cell is computed using a relation that includes only existing values. Therefore each unknown will appear in only one equation in the system and the equations for the unknown value in each cell can be solved one at a time to give the unknown quantities.*

On the other hand, *The pressure-based solver employs an algorithm which belongs to a general class of methods called the projection method. In the projection method, wherein the constraint of mass conservation (continuity) of the velocity field is achieved by solving a pressure (or pressure correction) equation. The pressure equation is derived from the continuity and the momentum equations in such a way that the velocity field, corrected by the pressure, satisfies the continuity. Since the governing equations are nonlinear and coupled to one another, the solution process involves iterations wherein the entire set of governing equations is solved repeatedly until the solution converges:*

For the Coupled formulation:

1. *Update fluid properties (e,g, density, viscosity, specific heat) including turbulent viscosity (diffusivity) based on the current solution.*
2. *Solve, simultaneously, a system of the momentum equations and pressure-based continuity equations.*
3. *Correct face mass fluxes, pressure, and the velocity field using the pressure correction obtained from Step 3.*
4. *Solve the equations for additional scalars, if any, such as turbulent quantities, energy, species, and radiation intensity using the current values of the solution*

      variables.
5. *Update the source terms arising from the interactions among different phases (e.g., source term for the carrier phase due to discrete particles).*
6. *Check for the convergence of the equations.*

Using density based solver, at first sight, could be the best choice, due to the fact it was especially developed for compressible flow simulation.

However, solving continuity equation at the same time of energy equation could lead to instability, and it is exactly what happens (Figure 1.11).
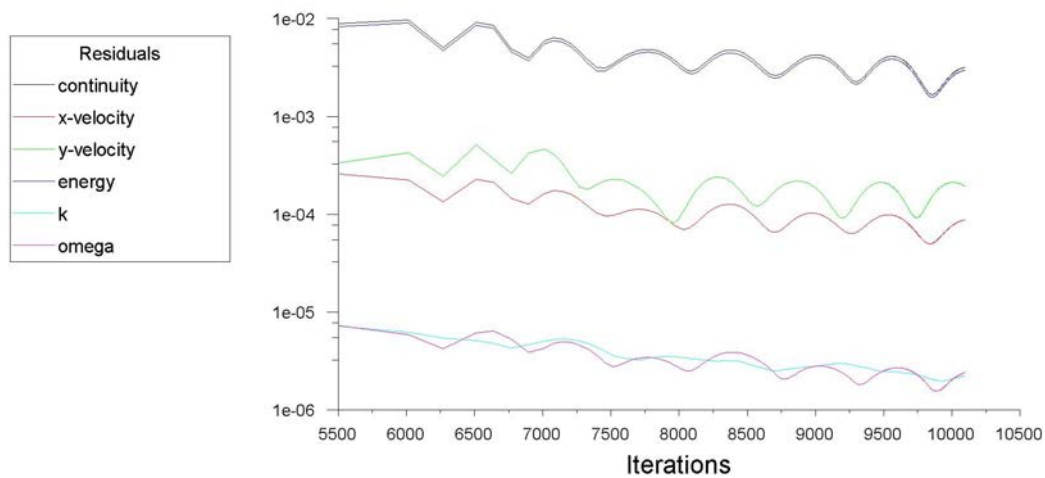
Figure 1.11: Residuals of convergence at first order by using density based solver

On the other hand, using pressure based solver, convergence at 1e-5 is reached at third order, using less than 2000 iterations (Figure 1.12 for reference).

The solution control parameters are:
- Courant Number: 50
- Explicit relaxation factors, Momentum: 0.35
- Explicit relaxation factors, Pressure: 0.35
- Under-relaxation factors, Density: 0.9
- Under-relaxation factors, Body Forces: 0.9
- Under-relaxation factors, Turbulent Kinetic Energy: 0.8
- Under-relaxation factors, Specific Dissipation Rate: 0.8
- Under-relaxation factors, Turbulent Viscosity: 0.95
- Under-relaxation factors, Energy: 0.95

From both Figure 1.11 and 1.12 it could be seen that turbulence convergence is guaranteed with both density based and pressure based approach, a sign that y+ settings are correct (Figure 1.13 for reference).

As example of simulation, in Figure 1.14 it is possible to see pressure distribution
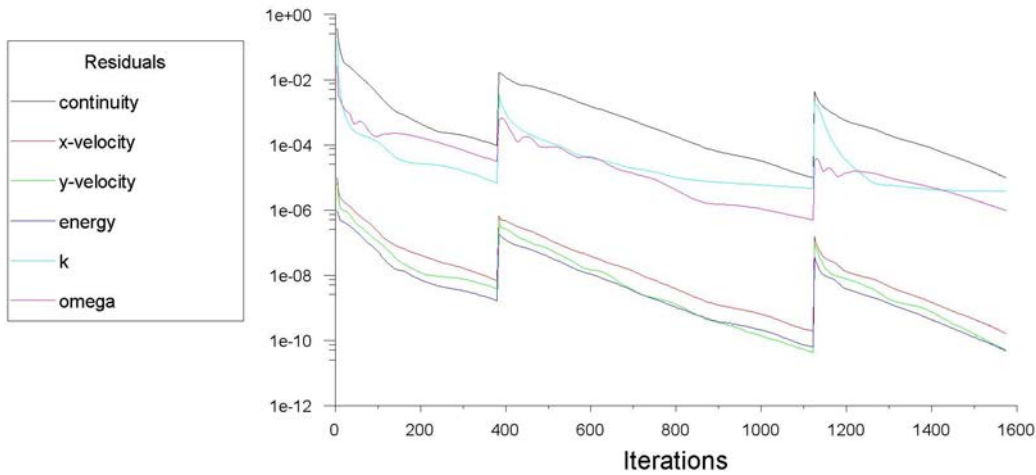
Figure 1.12: Convergence with Pressure Based Solver
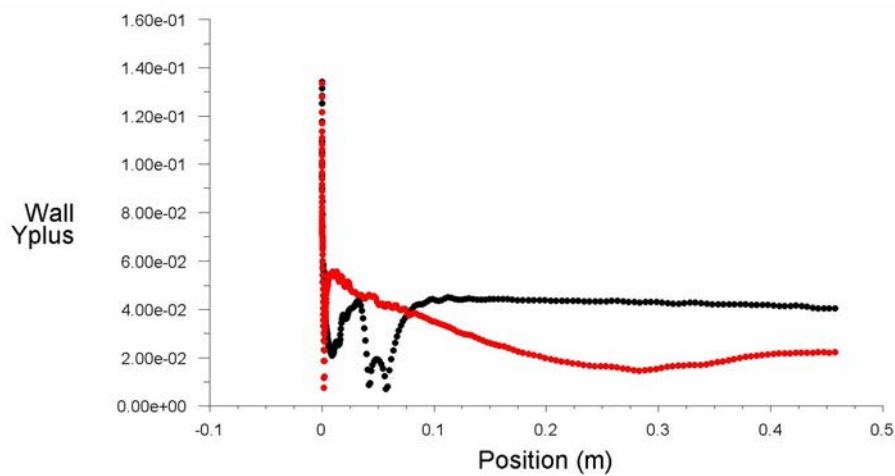
Figure 1.13: y+ distribution along inside and outside intake geometry: every value is under 1, perfect for k-w SST convergence

around the intake and streamlines.

It could be seen that streamlines have a divergent geometry, perfectly according with mass flow ratios: the engine is inspiring air at a mass flow that is half than the in-design one (which is 41.2 kg/s at this Mach number).

In Figure 1.15, contour of Total Pressure shows that, at the inner side, in pressure performance consideration, the influence of friction is limited to the boundary layer: in fact, total pressure, which must preserve its value during an isentropic process, is influenced by friction losses, and so by non-isentropic phenomena, only inside the boundary layer, and these influences doesn't compromise pressure efficiency during intake process (as long as fluid detachment is not present: in that case, total pressure drop could be much more noticeable).

24
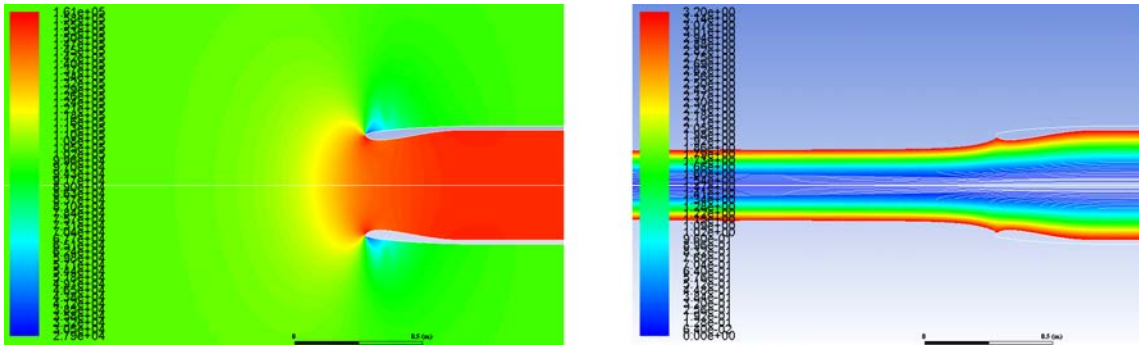
Figure 1.14: Contour at Mach = 0.84 and Mass Flow = 20 kg/s: on the left, pressure distribution around the intake, with the peak values at stagnation point at lip and at the intake surface; on the right, streamlines entering the intake.
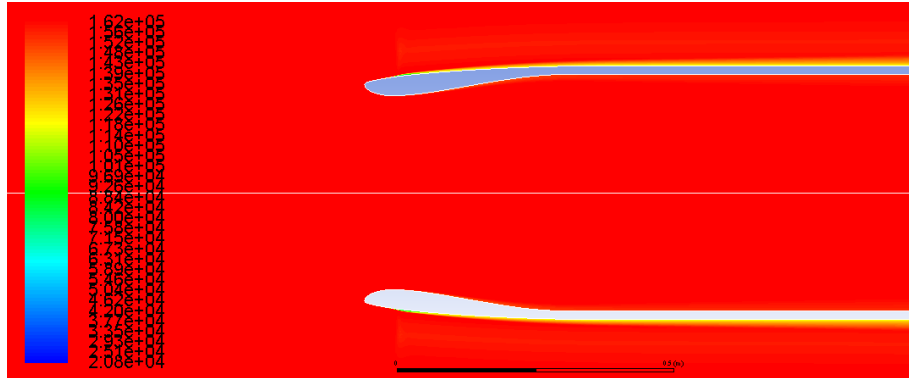
Figure 1.15: Contour of Total pressure around the intake at Mach = 0.84 and Mass Flow = 20 kg/s

On the other hand, it could be seen that, because of the high speed of the airflow, sonic transitions at the outer side cause total pressure drops around boundary layer. These phenomena will be taken into consideration when the optimization process will take place in last chapter, when drag performance reduction will be considered as a fundamental parameter of the overall performance of a subsonic intake.

1.2.4   Simulation

In order to validate experimental data, a series of simulation is now ready to be executed: Mach = 0.84 and three different mass flow ratios are the main boundary conditions of this set. After this first set, other simulations will be executed in order to improve model solidity and to find limits.

Chocking

Another datum which is fundamental to understand in these kind of phenomena is the mass flow at chocking, which is the situation where flow speed at the axis reaches

the speed of sound (the axis is taken as reference because, in two dimensions, sonic transitions could take place around inner edges of the intake at the thinner section without get to a complete sonic transition of the entire mass flow). Because of the high mass flow ratio in which wind tunnel tests were conducted, the CFD model must ensure that those values are possible to be reached, because many data in the report, as the temperature for example, are absent, and so this verification is compulsory in order to better predict flow behaviour at high mass flow.

A good way to predict mass flow at chocking, when the forcing quantity is a combination of flight speed and air intake, is to set mass flow boundary as a pressure outlet, with a static pressure equal or lower than the atmospheric one.

In this way, the intake behaves as a nozzle, and so ensuring to reach sonic transition at its thinner section.

This test was conducted for several Mach number. The solver utilized was a third-order one ((MUSCL as it's called in fluent), because first order is not precise enough for this kind of data searched.
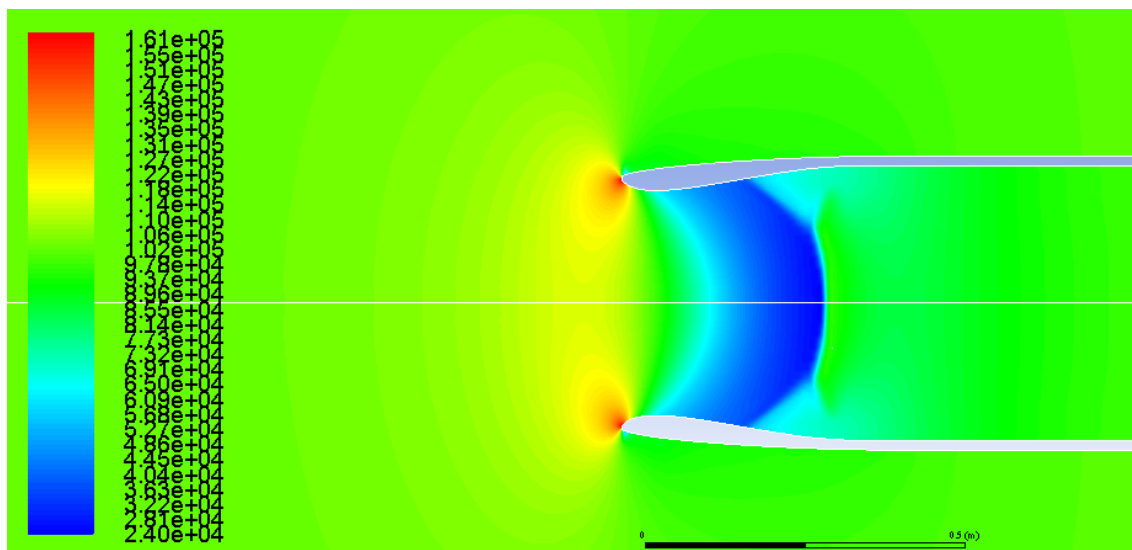
Figure 1.16: Chocking mass flow (33.23 Kg/s) at M = 0.84 (pressure contour)

The following data are the results of this investigation:

Mach number	Mass Flow [kg/s]	MFR
0.79	31.82	0.82102
0.84	33.23	0.80632
0.87	34.14	0.79977
0.89	34.77	0.79639
0.92	35.76	0.79234

MFR (mass flow ratio) is the ratio between the mass flow at highlight section, in which speed and density are the far-field ones, and the current mass flow.

So:

$$MFR = \frac{\dot{m}}{\rho_\infty A_{hl} M_\infty \sqrt{kRT_\infty}} \quad (1.8)$$

MFR is the given value of mass flow in the NASA report, so it is fundamental understanding the meaning in order to best set boundary conditions.
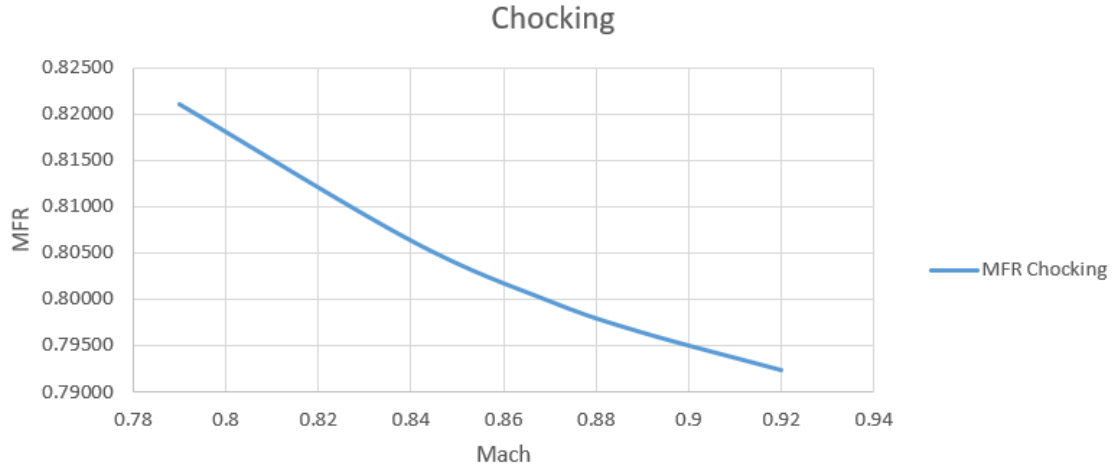
Figure 1.17: MFR at chocking for different Mach number at far-field

In the following subsection, it will be clearer why this calculus was done.

1.2.5 Simulation Run

For M = 0.84, a set of different MFR was selected, in order to compare results at low, medium and high mass flow.
MFR = 0.49, 0.67 and 0.84 were selected. However, the last one was impossible to simulate, because its mass flow is quite greater than the chocking one, but it will be run with the other only as a reference, to better understand the problems CFD faces during an impossible-physical situation, and to compare the results with the corresponding wind tunnel data.
For a better quality of the results, CFD was set to simulate with a solver, firstly, set at first order, then at second and third order. In fact, first order solver erases all the numeric instabilities and under-estimate, as it was seen during chocking mass flow calculus, the corresponding results, also in term of pressure recovery, which is the most important parameter for this thesis.
First of all, it was set a hybrid initialization, which lets the mesh to start the simulation with the quantities nearer to the ending solution, by using boundary condition as a reference (instead of standard initialization, which starts the simulation with the same values in each zone of the mesh)
Secondly, a complete first order simulation runs until convergence at 1e-5 is reached. At the end, second and third order solvers take simulation to the complete and most accurate convergence.

1.3   Validation Results

Once every simulation run ended, results are written in a .xy file in term of pressure coefficient

$$Cp \; = \; \frac{2}{kM_\infty^2}\left(\frac{p}{p_\infty}-1\right) \tag{1.9}$$

on y axis and x axis length oriented. Pressure coefficient is plotted on intake's wall boundaries. Data are then compared to wind tunnel tests data by plotting graphs in a post processing elaboration made up by Microsoft Excel.
In Figures 1.18, 1.19 and 1.20 the complete results at Mach = 0.84.
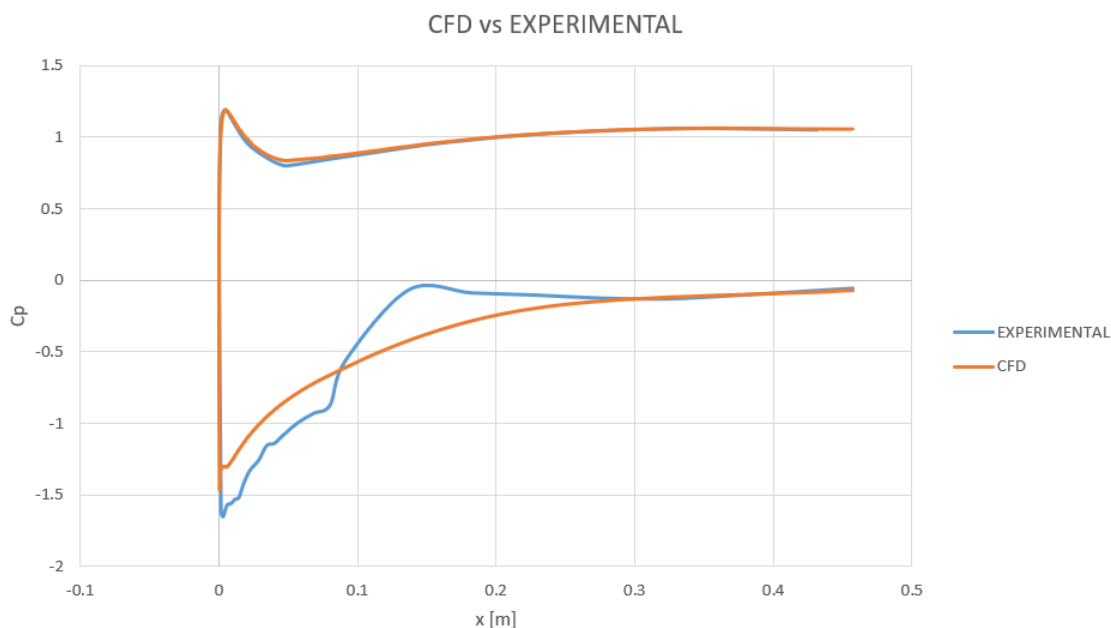
Figure 1.18: Cp comparison between experimental data from wind tunnel test and CFD simulation for MFR = 0.49 and M = 0.84

As figures above show, MFR = 0.49 and MFR = 0.67 lead to results very close to the experimental ones, and that's a sign of the model quality, a very good start for the optimization process that will take place in the last chapter.
On the other hand, last figure shows results completely different between experimental and CFD: in fact, Cp curve for wind tunnel test shows an acceleration of the flow that overcomes far-field speed (cp becomes negative), a clear sign of a sonic transition, located and bounded at thinner section of the intake, instead a complete sonic transition in the whole section of CFD results. The consequently continuous oscillation of cp values are caused by shock and boundary layer detachment.
In Figure 1.21 a comparison between streamlines of the three situation at different MFR.
In order to demonstrate that this CFD model is solid enough to simulate many different conditions of flight, another set of data was included in the investigation. In particular, first Mach number and MFR in which this intake was tested in wind tunnel: Mach = 0.79 and MFR = 0.61, 0.67 and 0.74. Higher values of Mach number
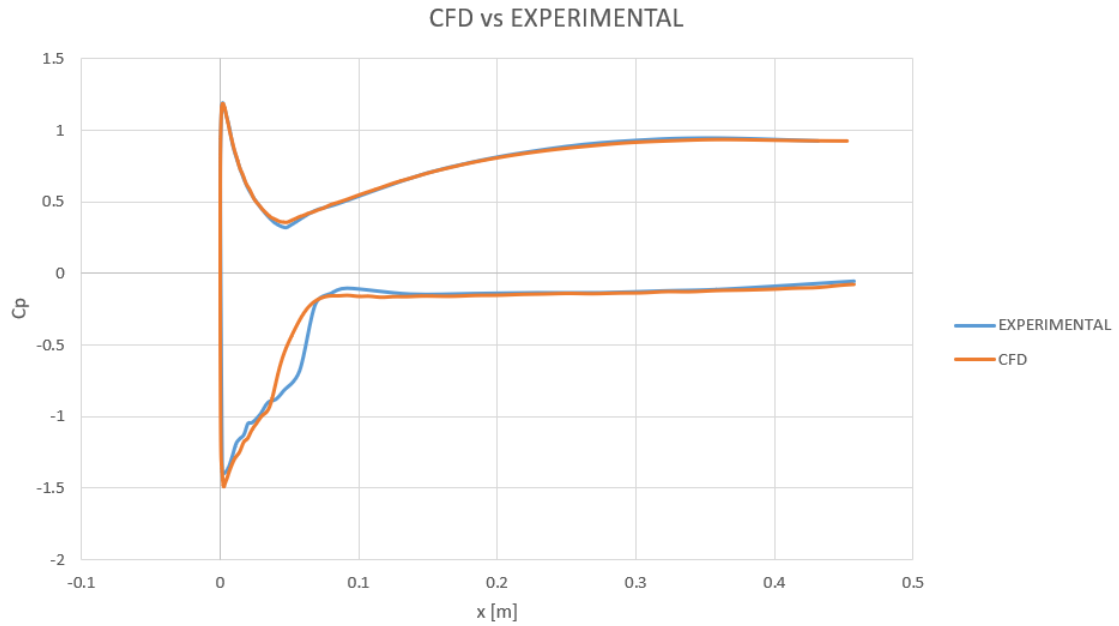
Figure 1.19: Cp comparison between experimental data from wind tunnel test and CFD simulation for MFR = 0.67 and M = 0.84
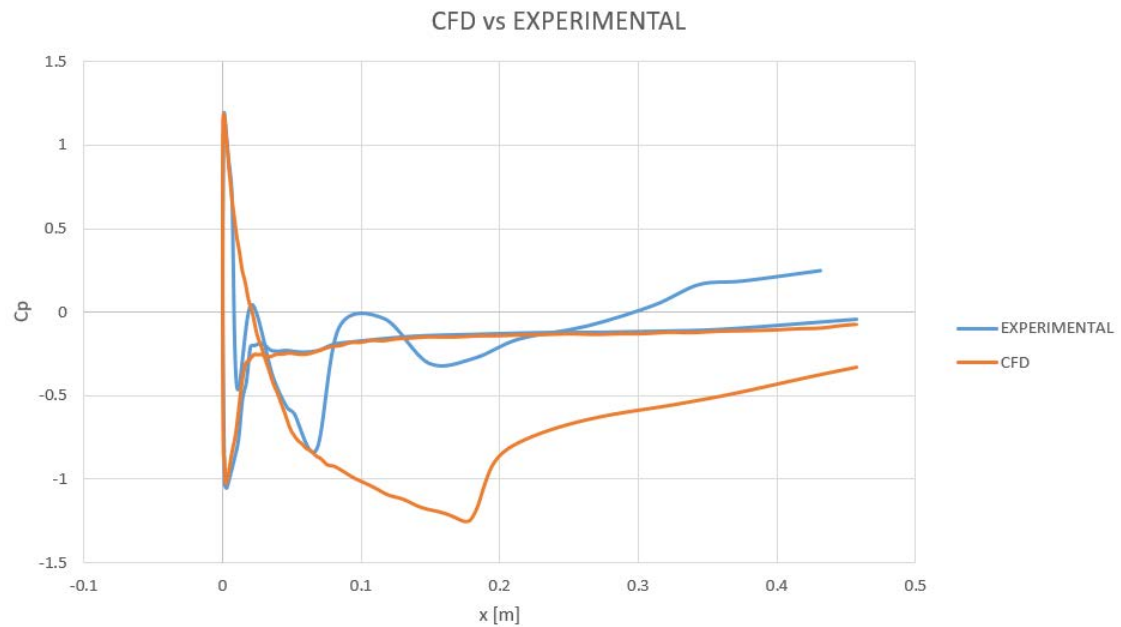
Figure 1.20: Cp comparison between experimental data from wind tunnel test and CFD simulation for MFR = 0.84 and M = 0.84

are not interesting because the physical situation enters in transonic flow and it will be impossible to evaluate a proper 1-dimension formulation to be compared with. The simulation process follows same steps of previous set.
Results in terms of pressure coefficient at intake's wall boundaries are reported in Figure 1.22, 1.23 and 1.24.
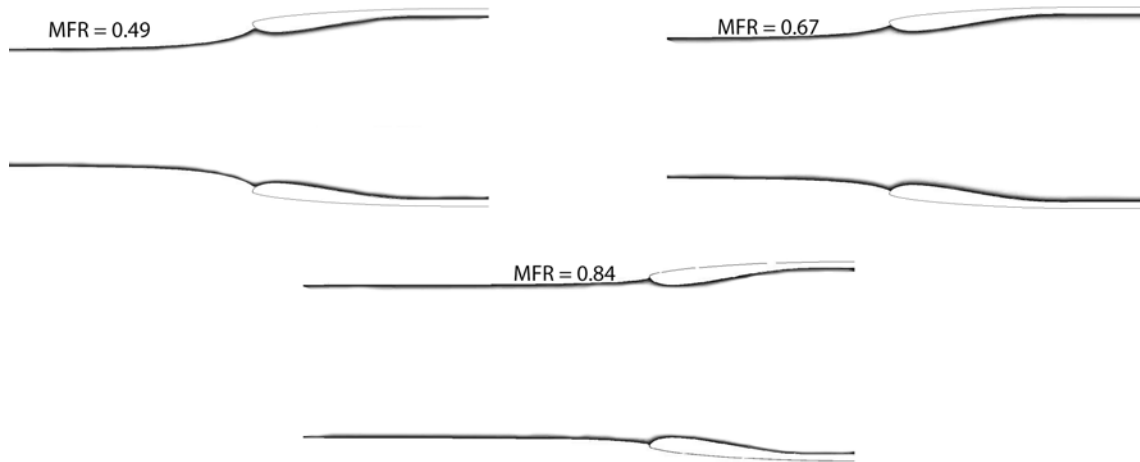
Figure 1.21: Streamlines dimensions at different mass flow ratio, M = 0.84
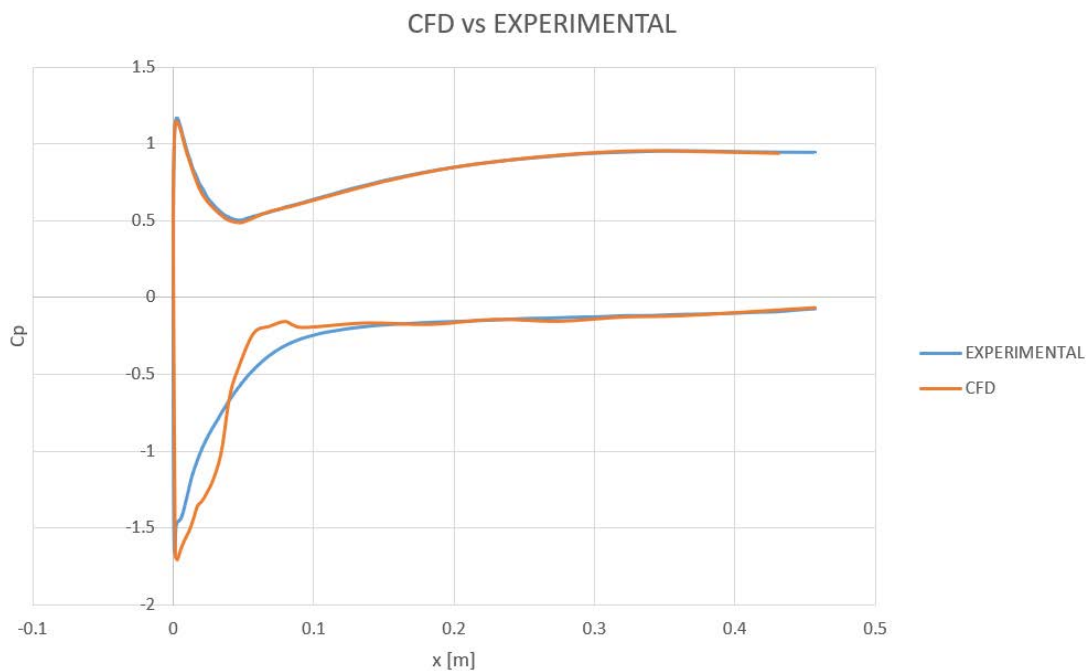
Figure 1.22: Cp comparison between experimental data from wind tunnel test and CFD simulation for MFR = 0.61 and M = 0.79

With this set, the CFD model results more precise than the other: an explanation could be given thinking about the lower Mach number at far field: in fact, this time, sonic transitions at outer sides are less intense, and so the consequent shock waves are less heavy for the solver processor.
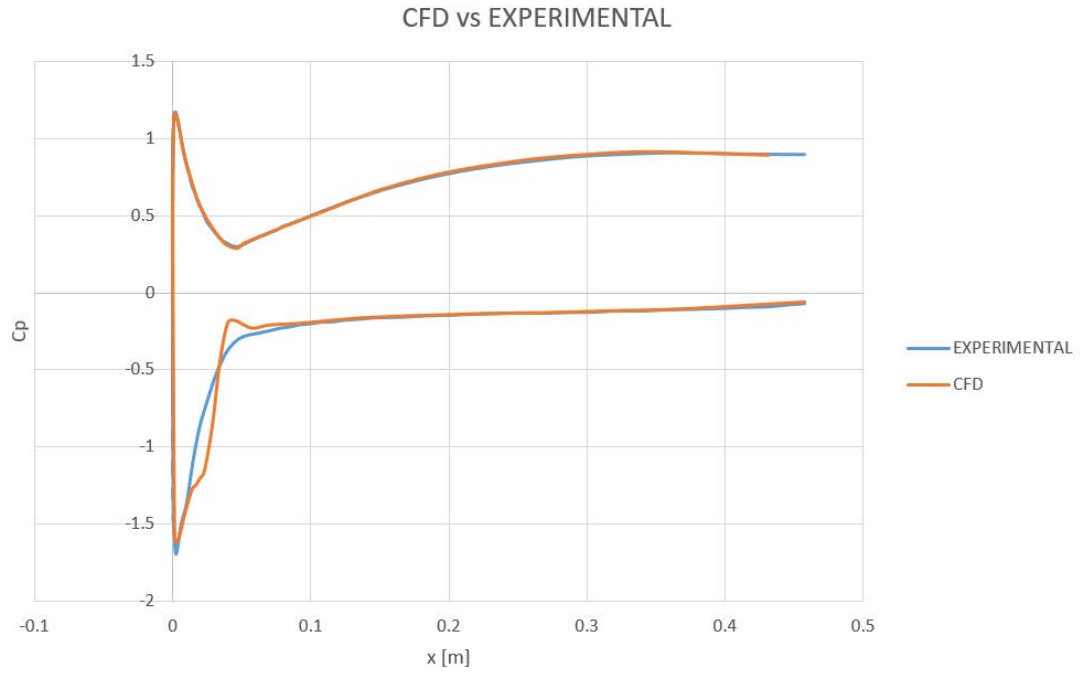
Figure 1.23: Cp comparison between experimental data from wind tunnel test and CFD simulation for MFR = 0.67 and M = 0.79
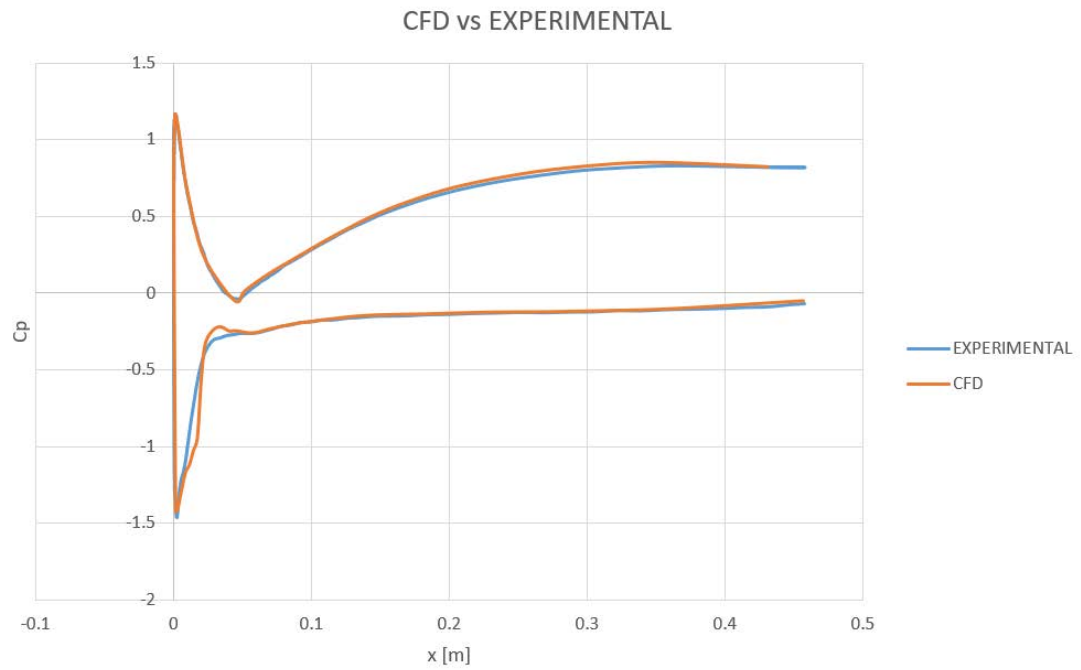
Figure 1.24: Cp comparison between experimental data from wind tunnel test and CFD simulation for MFR = 0.74 and M = 0.79

Chapter 2

1-D model

In order to understand in the best way the behaviour of the air entering the intake of an engine, a CFD model is the smartest method to reach this goal. However, a CFD model implies long time due to complex calculus process software has to accomplish, so a simpler method, maybe less precise, could get to a better engineering solution, especially for the first approach to the problem. Generalized Gas-Dynamics, developed in only one dimension (the axis of a duct), could lead to solutions that are very close to the real 3-dimensions ones, especially for long duct, in which the radial quantities are less important than the axial.

Also, 1-D and 3-D model have in common the formulation of continuity equation, which gives the limit of application for the intake (chocking mass flow for example) and gives, as consequence of generalized Bernoulli principle, to the same averaged values of pressure, temperature and velocity at the end of the intake geometry, without considering losses caused by non-isentropic phenomena like friction and shocks.

2.1   Concept

The first thing to take into consideration is the main approach to follow during the development of the code (in MATLAB): 1-d gas-dynamics allows the use of beginning and ending section to solve equations, without considering the geometry of the path air follows while moving. So, it is possible to know exactly the value of all the quantities at the end of the intake without the use of it's geometry.

However, if the value of thrust produced by the intake wants to be compared with the value extracted from CFD, the geometry of the intake becomes suddenly more necessary to 1-D considerations, even if end values will be the same. Thrust will be calculated in two different way:

1. Difference of Impulse Function calculated at the beginning and ending section;
2. Integrating pressure along intake wall and projecting the results on x-direction.

These values (which must be equal) will be compared to the those calculated in Fluent but post-processed in MATLAB by CFD pressure distribution results.

2.2   Diverging Streamlines

So, starting from boundary conditions, the first thing to be calculated is the compression of the air before entering the intake: In fact, the ram effect is caused by diverging shape that characterized streamlines due to a mass flow ratio lower than the cylinder-like one.
Knowing all the quantities at far-field, first thing to be computed is the starting section ("far away" from the intake):

$$A_\infty \; = \; MFR * A_{hl} \tag{2.1}$$

where A_{hl} is the area of highlight section of the intake.
After that, the area equation to calculate Mach number at the highlight section:

$$\frac{A_\infty}{A_{cr}} \; = \; \frac{1}{M_\infty} \sqrt{\left[\frac{2 \left(1 + \frac{k-1}{2} M_\infty^2 \right)}{k+1} \right]^{\frac{k+1}{k-1}}} \tag{2.2}$$

This allows to calculate the value of area at critic section (when M = 1) A_{cr}.
In this way, it is possible to calculate M_{hl} by knowing A_{hl} and A_{cr}:

$$\frac{A_{hl}}{A_{cr}} = \frac{1}{M_{hl}} \sqrt{\left[\frac{2 \left(1 + \frac{k-1}{2} M_{hl}^2 \right)}{k+1} \right]^{\frac{k+1}{k-1}}} \quad \Rightarrow M_{hl} \tag{2.3}$$

So, now it is possible to know all the quantities at the entrance of intake geometry:

$$p_{hl} \; = \; p_\infty \left(\frac{1 + \frac{k-1}{2} M_\infty^2}{1 + \frac{k-1}{2} M_{hl}^2} \right)^{\frac{k}{k-1}} \tag{2.4}$$

$$\rho_{hl} \; = \; \rho_\infty \left(\frac{1 + \frac{k-1}{2} M_\infty^2}{1 + \frac{k-1}{2} M_{hl}^2} \right)^{\frac{1}{k-1}} \tag{2.5}$$

$$T_{hl} = T_{\infty} \frac{1 + \dfrac{k-1}{2}M_{\infty}^2}{1 + \dfrac{k-1}{2}M_{hl}^2} \qquad (2.6)$$

For simplicity reason, the section of the diverging flux will grow linearly.

2.3 The Intake

The intake geometry, inside MATLAB, is processed by a b-spline function, which allow to increase the number of sample point from 64 (from reference) to 410 200, with $dx = 1e - 6$.
Only pressure side will be computed (suction/outer side in useless for 1-D calculus).
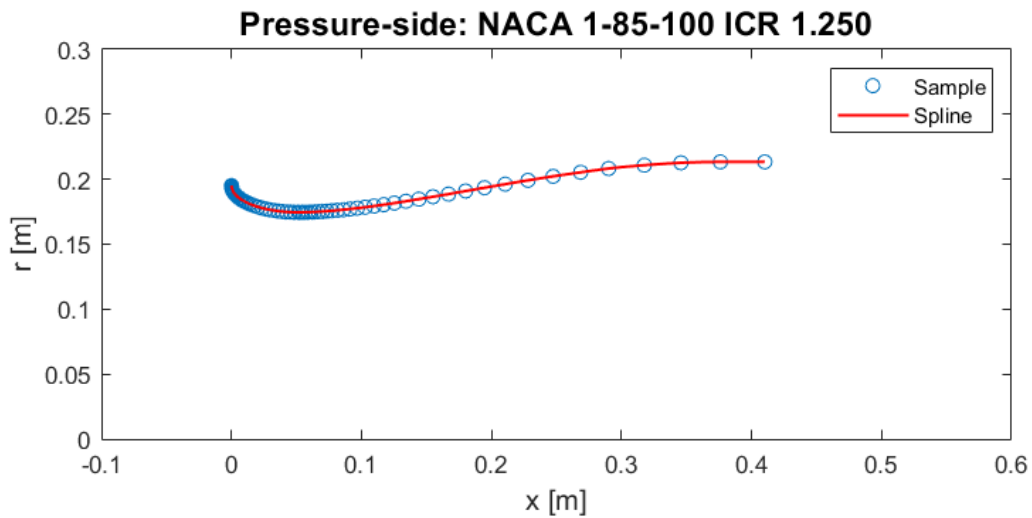
Figure 2.1: Spline development of the pressure/inner side of the intake geometry

Once entered the intake, quantities are integrated by a self-developed integrating function, a simpler way to evaluate quantities through the duct. Because of the large amount of sample point, an easy-to-evaluate histogram-like integrating method is the perfect choice for this purpose.

Equations are derived by influence-coefficient table of gas dynamics, with the only forcing-action of area.

To evaluate firstly Mach number through the duct:

TABLE 8.2
INFLUENCE COEFFICIENTS FOR CONSTANT SPECIFIC HEAT AND MOLECULAR WEIGHT

	$\dfrac{dA}{A}$	$\dfrac{dT_0}{T_0}$	$4f\dfrac{dx}{D} + \dfrac{dX}{\frac{1}{2}kpAM^2} - 2y\dfrac{dw}{w}$	$\dfrac{dw}{w}$
$\dfrac{dM^2}{M^2}$	$-\dfrac{2\left(1+\frac{k-1}{2}M^2\right)}{1-M^2}$	$\dfrac{(1+kM^2)\left(1+\frac{k-1}{2}M^2\right)}{1-M^2}$	$\dfrac{kM^2\left(1+\frac{k-1}{2}M^2\right)}{1-M^2}$	$\dfrac{2(1+kM^2)\left(1+\frac{k-1}{2}M^2\right)}{1-M^2}$
$\dfrac{dV}{V}$	$-\dfrac{1}{1-M^2}$	$\dfrac{1+\frac{k-1}{2}M^2}{1-M^2}$	$\dfrac{kM^2}{2(1-M^2)}$	$\dfrac{1+kM^2}{1-M^2}$
$\dfrac{dc}{c}$	$\dfrac{\frac{k-1}{2}M^2}{1-M^2}$	$\dfrac{\frac{1-kM^2}{2}\left(1+\frac{k-1}{2}M^2\right)}{1-M^2}$	$-\dfrac{k(k-1)M^4}{4(1-M^2)}$	$-\dfrac{\frac{k-1}{2}M^2(1+kM^2)}{1-M^2}$
$\dfrac{dT}{T}$	$\dfrac{(k-1)M^2}{1-M^2}$	$\dfrac{(1-kM^2)\left(1+\frac{k-1}{2}M^2\right)}{1-M^2}$	$-\dfrac{k(k-1)M^4}{2(1-M^2)}$	$-\dfrac{(k-1)M^2(1+kM^2)}{1-M^2}$
$\dfrac{d\rho}{\rho}$	$\dfrac{M^2}{1-M^2}$	$-\dfrac{1+\frac{k-1}{2}M^2}{1-M^2}$	$-\dfrac{kM^2}{2(1-M^2)}$	$-\dfrac{(k+1)M^2}{1-M^2}$
$\dfrac{dp}{p}$	$\dfrac{kM^2}{1-M^2}$	$-\dfrac{kM^2\left(1+\frac{k-1}{2}M^2\right)}{1-M^2}$	$-\dfrac{kM^2[1+(k-1)M^2]}{2(1-M^2)}$	$-\dfrac{2kM^2\left(1+\frac{k-1}{2}M^2\right)}{1-M^2}$
$\dfrac{dp_0}{p_0}$	0	$-\dfrac{kM^2}{2}$	$-\dfrac{kM^2}{2}$	$-kM^2$
$\dfrac{dF}{F}$	$\dfrac{1}{1+kM^2}$	0	$\dfrac{kM^2}{2(1+kM^2)}$	0
$\dfrac{ds}{c_p}$	0	$1+\frac{k-1}{2}M^2$	$\dfrac{(k-1)M^2}{2}$	$(k-1)M^2$

NOTE: Each influence coefficient represents the partial derivative of the variable in the left-hand column with respect to the variable in the top row; for example

$$\frac{dM^2}{M^2} = -\frac{2\left(1+\frac{k-1}{2}M^2\right)}{1-M^2}\frac{dA}{A} + \frac{(1+kM^2)\left(1+\frac{k-1}{2}M^2\right)}{1-M^2}\frac{dT_0}{T_0} + \frac{kM^2\left(1+\frac{k-1}{2}M^2\right)}{1-M^2}\left(4f\frac{dx}{D}+\frac{dX}{\frac{1}{2}kpAM^2}-2y\frac{dw}{w}\right)$$
$$+\frac{2(1+kM^2)\left(1+\frac{k-1}{2}M^2\right)}{1-M^2}\frac{dw}{w}$$

Art. 8.4

FLOW WITH CONSTANT c_p AND w

231

Figure 2.2: Influence coefficients table for constant specific heat and molecular weigth from *The Dynamics and Thermodynamics of Compressible Fluid Flow Vol.1 by Ascher H. Shapiro, Pag 231*

$$\frac{dM^2}{dx}(j) = M^2(j)\frac{2\left(1+\dfrac{k-1}{2}M^2(j)\right)}{M^2(j)-1}\frac{1}{A(j)}\frac{dA}{dx}(j) \qquad (2.7)$$

$$M^2(j+1) = M^2(j) + \frac{dM^2}{dx}(j)dx \qquad (2.8)$$

Once calculated the distribution of Mach number, it is possible to evaluate pressure, temperature and density:

$$\frac{dp}{dx}(j) = p(j)\frac{kM^2(j)}{1-M^2(j)}\frac{1}{A(j)}\frac{dA}{dx}(j) \qquad (2.9)$$

$$p(j+1) = p(j) + \frac{dp}{dx}(j)dx \qquad (2.10)$$

$$\frac{dT}{dx}(j) \ = \ T(j)\frac{(k-1)M^2(j)}{1-M^2(j)}\frac{1}{A(j)}\frac{dA}{dx}(j) \tag{2.11}$$

$$T(j+1) \ = \ T(j) + \frac{dT}{dx}(j)dx \tag{2.12}$$

$$\frac{d\rho}{dx}(j) \ = \ \rho(j)\frac{M^2(j)}{1-M^2(j)}\frac{1}{A(j)}\frac{dA}{dx}(j) \tag{2.13}$$

$$\rho(j+1) \ = \ \rho(j) + \frac{d\rho}{dx}(j)dx \tag{2.14}$$

Results are plotted from section at far-field up to the intake's last one.
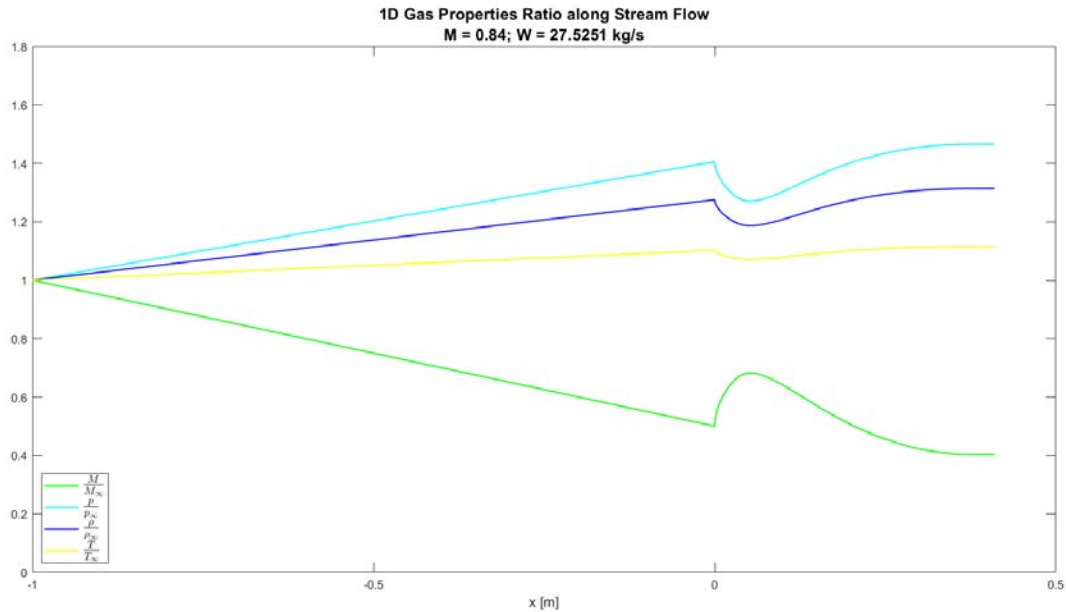
Figure 2.3: Ratios between quantities along flow-tube and intake and at far-field. M = 0.84; MFR = 0.67

From Figures 2.3 and 2.4 it could be seen, as obvious, that quantities copy perfectly the geometry of the intake, and this is because of the absence of radial 2-d effects on flow.
A comparison, at this point, between 1-D solutions and CFD 2-D axisymmetric is necessary for a "validation" test of this model.

- Mach number: MATLAB gives a final value of 0.34, whereas Fluent result is 0.36, with a percentage difference of 5.7%;
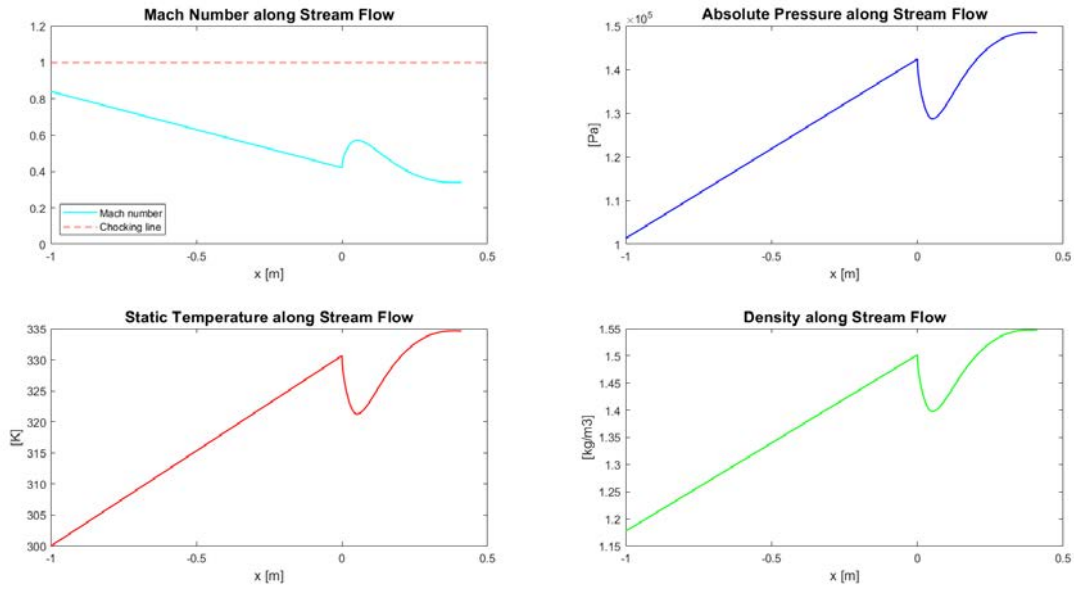
Figure 2.4: Real values of Mach number, pressure, temperature and density along flow-tube and intake.
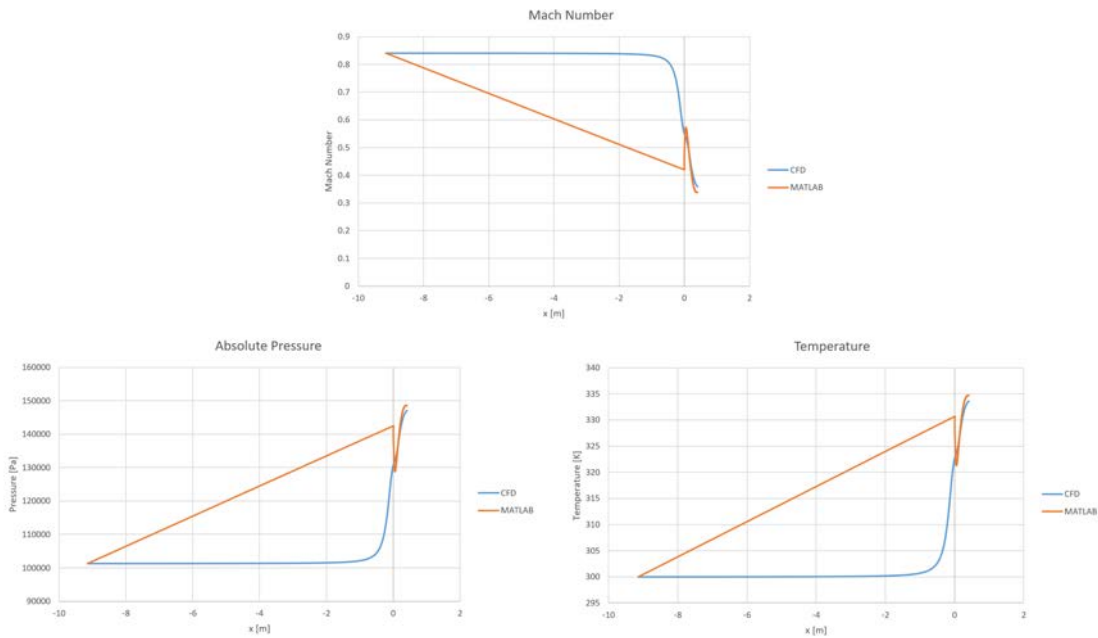
Figure 2.5: Comparison between MATLAB 1-D solutions and CFD at Mach = 0.84 and MFR = 0.67

- Pressure: MATLAB gives a final value of 148544 Pa, whereas Fluent result is 147069 Pa, with a percentage difference of 1%;

- Temperature: MATLAB gives a final value of 334.65 K, whereas Fluent result is 333.64 K, with a percentage difference of 0.3%.

Last results are the most important: the comparison between thrust produced by the increasing pressure inside the intake, evaluated in 1-D and 2-D axisymmetric. First of all, Fluent results are imported in MATLAB, in particular the pressure distribution along intake inner surface.

Force in x-direction is calculated by:

$$F_x = 2\pi \int_0^L rp\,dr \qquad (2.15)$$

Fluent pressure distribution returns a value of $F_{x,CFD} = 3100$ N.

With 1-D results, two different ways will be investigated:
  1. Direct calculus (like Fluent);
  2. Difference between Impulse Function, evaluated in first section and last section of the intake.
Second way is used with this equation:

$$F_x = p_{end}A_{end} + \rho_{end}A_{end}M_{end}\sqrt{kRT_{end}} - p_{hl}A_{hl} + \rho_{hl}A_{hl}M_{hl}\sqrt{kRT_{hl}} \qquad (2.16)$$

The results are the same, as expected, and return the value of: $F_{x,1D} = 3407$ N.

The difference between two formulations is of 9.9%.

In order to validate more accurately this 1-dimension model, it could be also useful to compute graphics, final quantities and thrust also for a different situation, and so same analysis of previous pages will take place too.
So, lowest Mach number data from tabulated wind tunnel results of this intake will be put under investigation: Mach number = 0.79 and MFR = 0.61.
Results are really comfortable, because confirm that 1-d and CFD 2-d axisymmetric are very similar.

In fact, percentage differences between two formulation are:
  • Mach number: MATLAB gives a final value of 0.30, whereas Fluent result is 0.32, with a percentage difference of 6.86%;

  • Pressure: MATLAB gives a final value of 143867 Pa, whereas Fluent result is 142524 Pa, with a percentage difference of 0.94%;

  • Temperature: MATLAB gives a final value of 331.61 K, whereas Fluent result is 330.67 K, with a percentage difference of 0.24%.

Graphic plots and comparison are reported in Figure 2.5
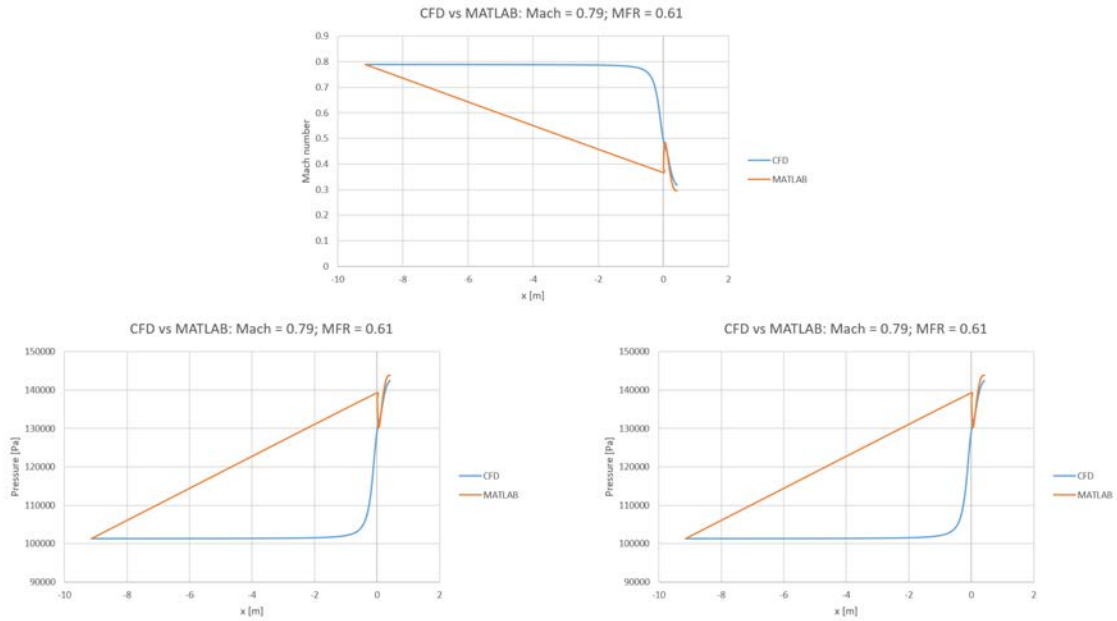
Figure 2.6: Comparison between MATLAB 1-D solutions and CFD at Mach = 0.79 and M = 0.61

Concerning thrust, Fluent pressure distribution get a value of $F_{x,CFD} = 3017.8\,N$, whereas MATLAB returns a value of $F_{x,1-D} = 3297.1\,N$, a difference of only 8.5%.

As a final statement, differences between 1-D Gas Dynamics formulation and CFD 2-D axisymmetric are mainly caused by the absence of boundary layer and quantities variation in radial direction in the second one.
This causes and higher isentropic compression for the 1-D formulation, and so, consequently, lower values of Mach number and higher values of pressure and temperature at the end of intake geometry.

Chapter 3

Optimization

The case study of this thesis is focused on an intake that was the results of years of tests, and it is especially designed for working at its maximum performance when flight speed is high subsonic, and so it's not wrong to think that the shape is already optimized for the purpose it was designed for.
In order to learn how much this intake geometry is suited for its purpose, why not trying to improve that (possible) optimization with another one, which starts after the actual geometry?

An optimization tries to improve some parameters that characterize a phenomenon by modifying some quantities that rule that particular physical question.

In mathematical language, the objective of an optimization is to find the minimum (or maximum) of a given function $O(\vec{x})$, where $\vec{x}$ is the vector of decisional variables. $\vec{x}$ could be, for example, the parametrization of a particular geometry; $O(\vec{x})$ could be a a function that that gives different results, like a vector function:

$$\begin{cases} O_1(\vec{x}) = ... \\ O_2(\vec{x}) = ... \\ O_3(\vec{x}) = ... \end{cases} \tag{3.1}$$

In particular, for aerodynamic phenomena, the physics is conditioned by the shape of geometries that identify airfoils and, in general, surfaces that are subjected to airflow. The function becomes now a vector that returns Coefficient of Lift (C_L), Coefficient of Drag (C_D), Coefficient of Moment (C_m), aerodynamic pole $P(x, y)$...

$$\begin{cases} O_1(\vec{x}) = C_L \\ O_2(\vec{x}) = C_D \\ O_3(\vec{x}) = C_m \\ O_4(\vec{x}) = P(x, y) \end{cases} \tag{3.2}$$

In this case, boundary conditions are fixed by the purpose of the intake: velocity, pressure, mass flow are not parameters that could change during optimization process, because they identify the intended use for this kind of geometry.

Also, all the boundary condition are set in order to compare results to the original shape, and so wind tunnel tests that gave birth to this thesis project.

In order, also, not to distort excessively the geometry of the intake, highlight area, mass flow inlet area and overall length will remain unmodified, so as to prevent the intake to admit much more air than it was capable of before.

Minimum section could vary, and also the thickness of the cowl could change during the process.

These limitations of course will influence severely results of optimization, but also reduce computational cost and the number of variables to be post processed.

In the end, this chapter will represent also a guide to conceive, create and run a quite simple optimization process, by using MATLAB, the pre and post processor of this analysis, Pointwise, the mesh-software, and Ansys Fluent, the solver.

All the process will be described in details, especially the creation and manipulation of the intake shape, which represents first obstacle to be overcome.

3.1   Concept

In mathematical analysis, so as to find the minimum (or maximum) of a function, the process involves derivatives and gradients: in fact, those points in which derivatives are equal to zero are the same point in which the function could have a local (or global, it depends on the shape of the function) minimum (or maximum). When more than only one variable determines function behaviour, the attention focuses on the differentiation of a the function: derivation process involves either the variables, and gradient vector is a sort of an indication for the direction to follow to reach minimum (or maximum).

In this case, instead of one function with several variables, the are many function determined by same several variables: this is called Multi-objective Optimization.

In fact, a complex selection of operation determined by the shape of the airfoil lead to quantities that are, in some way, disconnected or, especially, in discord.

For example, in a wing, the shape of the airfoil and the angle of attack determine how much lift and drag force it could generate: in particular, lift and drag are quantities in opposition, because the first wants to be maximized, the second minimized, but one of the major source of drag is just the lift. So, in a optimization, if it's impossible to act on the angle of attack because it will worsen drag performance, maybe aspect ratio will be one detail to be focused on.

So, if it is impossible to reach a global minimum and a global maximum, because targets are in opposition, a compromise between them will be the only alternative.

For these reasons, the main result of the optimization the best compromise between two target variables, and it is called Pareto Front of the function.

So, how many objectives will be the targets of minimization (or maximization)?

An intake could be defined after its main purpose, to slow down airflow before entering te engine. At a given mass flow, to match flight speed to final air speed, pressure increases due to mass and momentum conservation. Main cause of this pressure in-
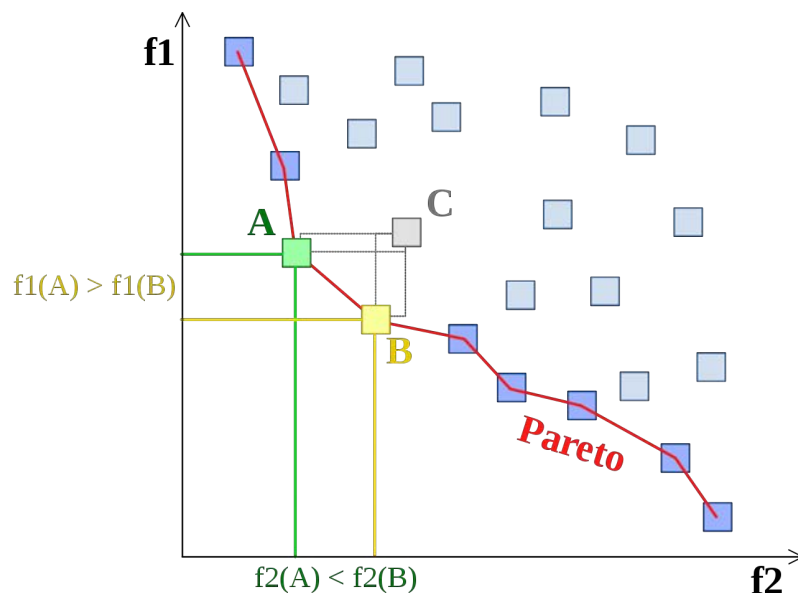
Figure 3.1: An example of Pareto front for two objectives (Author: Johann Dréo; Date: May, 9, 2006)

crease is the diverging shape of the intake, and so, setting up first and last section, as 1-dimension gas dynamics explains, pressure recovery will be fixed. In reality, when 3-dimensions quantities enter the simulation, fluid detachment, sonic transition and turbulent boundary layer ruin the perfect result.

So, two possible targets will be:
- minimizing the coefficient of drag C_D of the overall cowl geometry;
- maximizing average coefficient of pressure $\overline{C_P}$ at mass flow inlet;

In summary, the optimization takes the form as follows.
A function $C_D(\vec{x})$ turns the shape into drag coefficient values; another function, $\overline{C_P}(\vec{x})$, turns the shape into an averaged pressure coefficient.
The goal of the optimization is to find best compromise between lowest drag coefficient and maximum pressure recovery.

By analysing first chapter simulations, an important consideration comes to the attention: drag coefficient is negative. This kind of simulation investigates in airfoil performance without considering wake behaviour, because mesh field lies only around leading edge, whereas trailing edge doesn't exist, and inner and outer flow are completely separated. In fact, due to its shape, outer side of the intake tends to increase flow speed, leading to reduction of pressure acting on the body. So, drag performance could be seen as how much pressure reduction could the outer side perform on the flow.
Because of these considerations, in order to minimize drag coefficient, taking in consideration the absolute value of cd is wrong. The right choice becomes a maximization of the absolute value of drag, by minimizing $\frac{1}{|C_d|}$.

43

Another question could be: is this intake, which is designed for high subsonic flight, optimized for take off phase, in which mass flow and flight speed are much lower?
An answer could be given by reading *"A Complete Investigation of Three NACA 1-Series Inlets at Mach Numbers up to 0.92" by Richard J. Re and William K. Abeyounis of Langley Research Center, Hampton, Virginia*, the main source of data for this thesis: Low subsonic flight prefers smooth variation of geometry and rounded cowl lip, in order to prevent fluid detachment at low Reynolds number; High subsonic prefers a thinner outline for the intake, in order to increase chocking mass flow, and so prevent sonic transitions to reach the inlet of engine.
So, it will be mandatory to set up multiple boundary conditions simulations: every time the solver faces the new geometry, it simulates first at high subsonic speed (Mach = 0.84), after at low subsonic speed (Mach = 0.3, for example); mass flow will be varied only by the variation of Mach number at far-field, mass flow ratio (MFR) will remain the same.
At Mach = 0.84 and MFR = 0.67, the model was validated (previous chapters), and so the resulting data are suitable for a comparison.

3.2 Optimization technique: Genetic Algorithm

There are several ways to perform an optimization process, but when the shape of the fitness function is too complex to be evaluated in an analytic form (this case), a useful way to develop an optimization is setting up a genetic algorithm (GA): based on the behaviour of chromosomes across generations, a genetic algorithm performs on decisional variables and, by processing them, gives the results, known as "fitness": every combination of decisional variables, randomly on a user defined domain, has its own fitness, and a set of variables and fitness values is called population.
A population evolves during generations, and in the passage between one and another (the generation process), three main operations will be performed by the algorithm:

1. Selection
2. Crossover
3. Mutation

3.2.1 Selection

Based on fitness values, the GA selects individuals, for example, by using a "roulette technique": every set of variables and fitness is divided in most fitted and less fitted, and most fitted have a greater probability to be selected.
Selected individuals will perform a tournament, and only best fitted will pass to the next generation.

3.2.2 Crossover

Individuals with high fitness will cross their decisional variables, giving birth to other individuals with mixed characteristics (variables in this case).
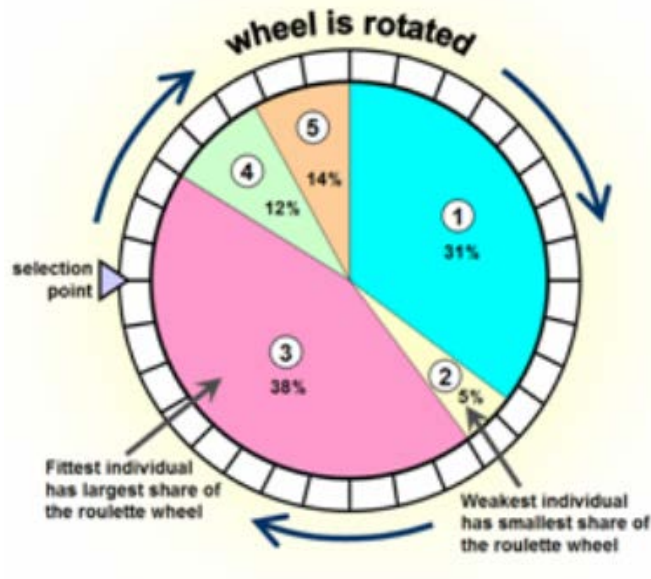
Figure 3.2: An example of how a "roulette technique" works

Crossover operates by several methods:
- Single Point
- Two Point
- Uniform
- Simplex

3.2.3 Mutation

A random modification of one variable of a selected individual.
The global effect is presented in Figure 3.4
The process continues until tolerance or generation limit is reached.
It is clear that the possibility of reaching the Pareto Front of the function increases with the number of generations, and so this will be an important consideration while choosing between computational cost and accuracy.

3.3 Process Set-up

Developing an optimization strategy from zero is quite difficult, especially for the large number of variables the function has to compute in order to understand the function behaviour, which represents the "skill" of the process.
Fortunately, MATLAB developed some embedded functions that suit perfectly for the purpose of this thesis. In particular, it was developed a genetic algorithm that, by performing on some decisional variables, executes the fitness function and get the results, all on its own.
The function *gamultiobj*, as the user guide explains, *x = gamultiobj(fun,nvars) finds x on the Pareto Front of the objective functions defined in fun. nvars is the dimension*
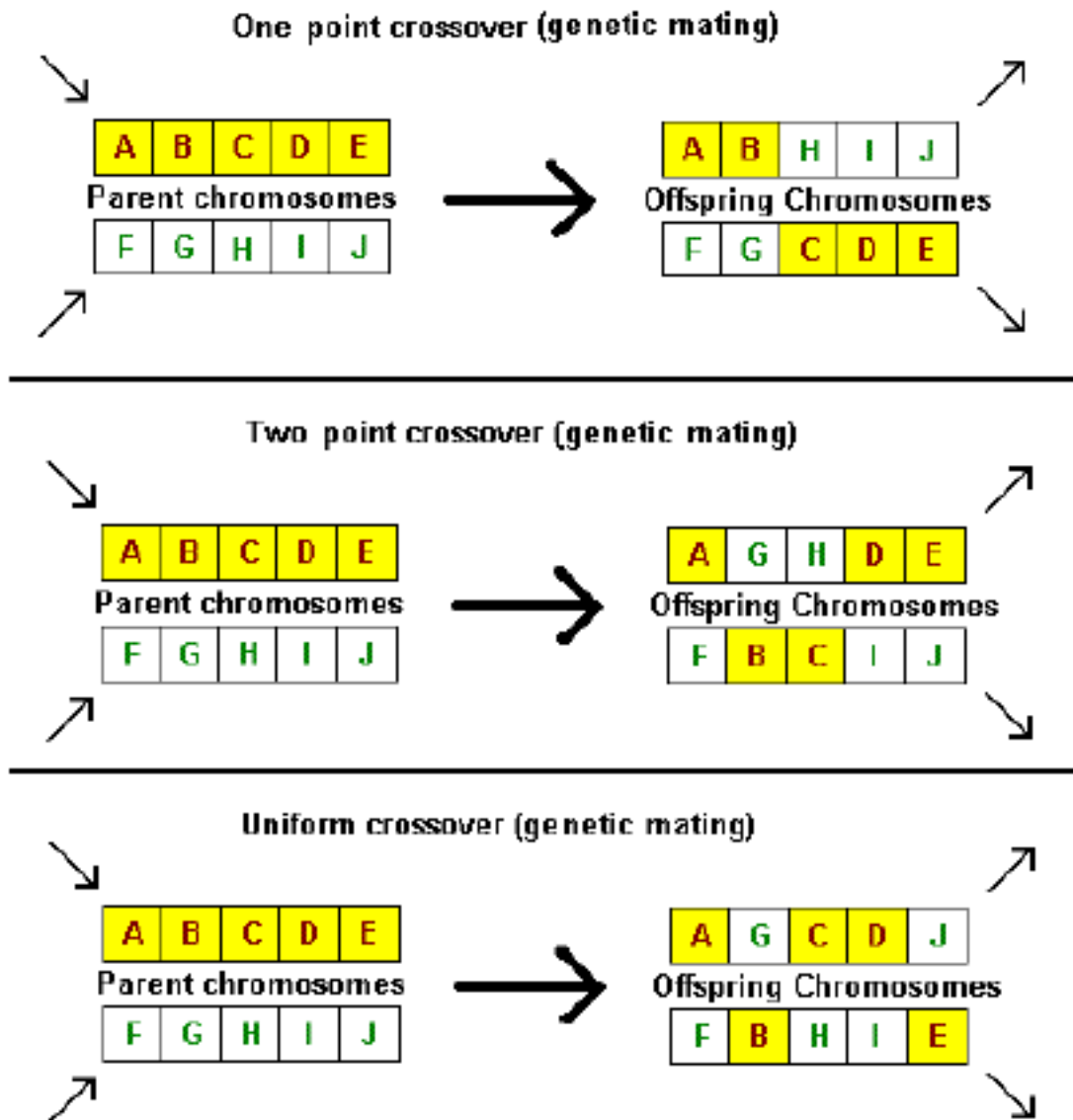
Figure 3.3: Example of Crossover process

of the optimization problem (number of decision variables). The solution x is local, which means it might not be on the global Pareto front. In fact, only a large number of function evaluation is able to understand if the Pareto Front is local or global. For the purpose of this thesis, several generations will be needed in order to reach the targets.

The fitness function, in this case, will contain all the information that, from a geometry, get to the fitness value, and MATLAB needs to be able to compute this function automatically. So, the software needed to mesh and perform the solution
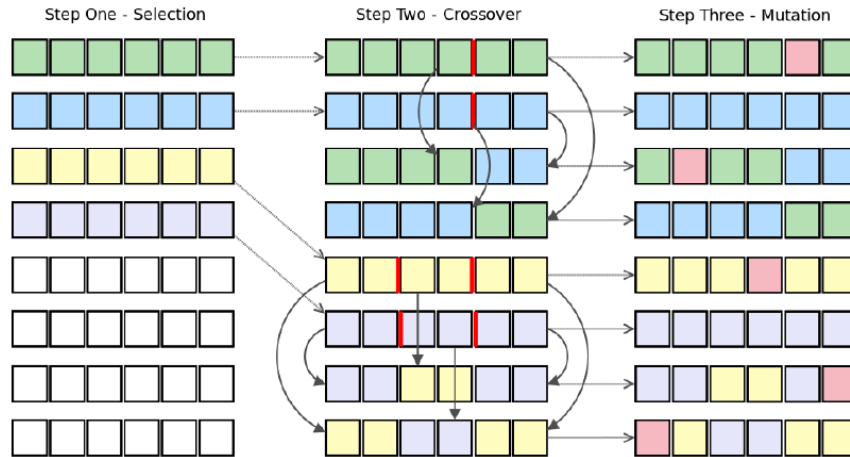
Figure 3.4: The global effect of a Genetic Algorithm

must receive commands by a command line, or more easily a journal file containing all the strings.

MATLAB is able to write journal file by simply writing instructions on text file. To start and execute the software, MATLAB uses command *system* to run in DOS mode, and so working in command prompt of Windows system. By this interface the software has embedded, the optimization process could run without any further undo: the script will be written considering both MATLAB language and Point-wise/Fluent ones.

Before writing the script, a useful way to draw an airfoil has to be find: in fact, it's quite difficult to optimize an aerodynamic shape by its spline control point, because, in order to obtain a proper resolution, thousands of point will be needed.

Fortunately, an airfoil could be easily parameterized by a Bezier Curve, which needs only few control point to be developed. By these curves, first the original airfoil of the intake could be retraced by a simple but really accurate overlap, and after the control point represents the decisional variables of the GA.

3.3.1   Bezier Curve

A Bezier curve is a parametric curve related to Bernstein polynomial.
It is defined by a set of control points P_0 to P_n, in which n is the order of the curve (n = 1 for linear, n = 2 for quadratic...). The first and the last point are always the extreme points of the curve.
The general expression is:

$$B(t) = \sum_{i=1}^{n} b_{i,n} P_i \tag{3.3}$$

in which
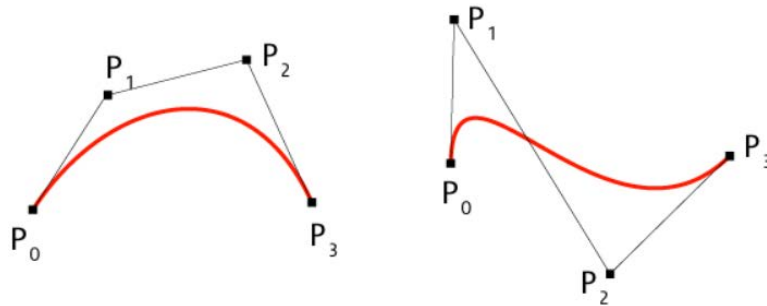
Figure 3.5: Examples of Bezier curves

$$b_{i,n} = \binom{n}{i}(1-t)^{n-i}t^i \qquad i = 0, ..., n \qquad (3.4)$$

are the Bernstein basis polynomials of degree n.

In MATLAB, the Bezier parametrization is made by creating, firstly, the Bernstein matrix, that returns a length(t)-by-(n+1) matrix B in which t is the vector t = 0,...,1.
To get the Bezier curve, multiply the matrix B by the matrix P of control point.
In this way, by several attempts, it is possible to fully overlap the airfoil.

In order to keep the tangency between two sides at leading edge, first two control point of each side has to be aligned. This is the same way to keep tangency to x-axis at trailing edge.
In this way, it is clear that, given 9 control points, for a total number of variables of 18, many of these will be left unchanged in order not to change overall length and highlight and mass flow inlet section.
For the suction side, a 3rd order Bezier curve was enough precise to overlap perfectly the original shape, because of its only one curvature, whereas in pressure side, due to two main curvatures, needs at least a 4th order curve.

At the end, the decisional variables, due to previous considerations, will be:

- suction side: y of 2nd point;
- suction side: x of 3rd point;
- pressure side: y of 2nd point;
- pressure side: x of 3rd point;
- pressure side: y of 3rd point;
- pressure side; x of 4th point;

So, the optimization will be done performing on 6 decisional variables.
Boundary constraints for the shape of the intake are chosen in order, at the extrema,
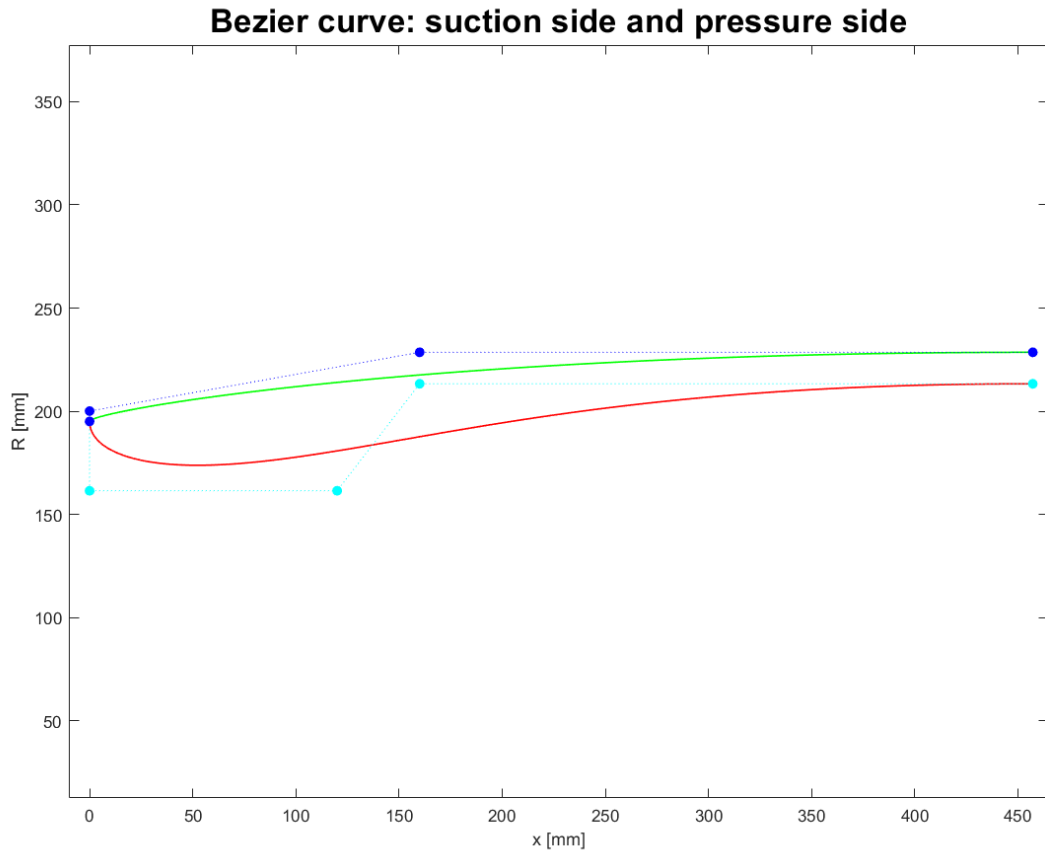
Figure 3.6: Result of Bezier parametrization of intake airfoil

to get a geometry thin enough at one side, thick enough at the other, so as cowl lip could vary from the sharpest to the smoothest edge (Figure 3.7).
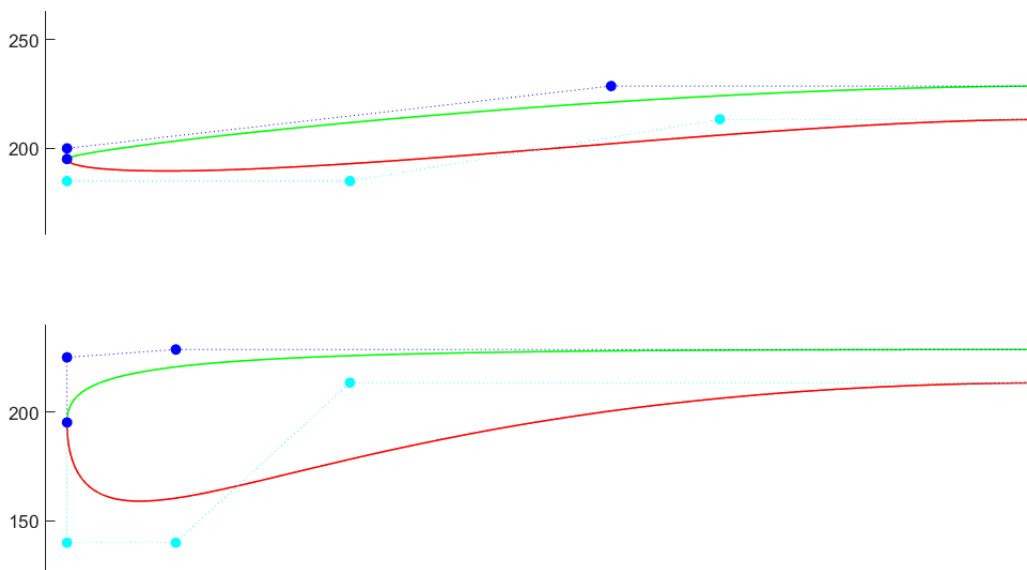
Figure 3.7: Extrema of intake shape by boundary constraints

3.3.2   Fitness Function

Pointwise

After having set up the decisional variables, the airfoil is ready to be uploaded on Pointwise. In order to maximize the resolution of the airfoil, which does not influence mesh resolution, the airfoil is approximated by 1000 sample points: this was implemented in the t vector dimension, from 0 to 1 with a step of 0.001. Next, once in the meshing software, the airfoil, firstly, needs to be converted in a connector. In order to load directly and in the simplest way the airfoil as a connector, its points will be directly put into the spline function parameters: in fact, in the form of Catmull-Rom, a sequence of point generates directly a continuous curve, which is split on the leading edge.
After that, airfoil is extended at trailing edges as in previous model.
Most important thing while creating a mesh domain, which could change after modifications on the mail shape, is to use a discretization of the connectors which remains unchanged even if dimensions in the airfoil distort too much: in fact, a structured mesh needs the connector to be composed by the same number of points at alternate sides. So, for example, if suction side change number of points as a consequence of a large change in the shape (just one point prevent the mesh to be created), also the connector at far-field needs to be modified, and that's too complicated in order to minimize computational time, the worst enemy of optimization process. As a consequence, the discretization of airfoil curve, after several attempts, is made up by a predetermined number of points, instead of a precise Δs. After that, a minimum Δs (spacing) is set so as to constrain the curve to have more points around the leading edge and less at trailing edge.
When all the boundaries are set up, the structured mesh is generated, in the same way as in previous chapters.
Last thing to compute before exporting the grid is to correct normals directions of every domain block and improve mesh quality, in terms of skewness angle and aspect ratio, by the optimization solver embedded.
After having set up boundary and volume condition, as well in previous chapters, the mesh grid is ready to be exported into a .cas file and to be read by Fluent.

Fluent

In fluent, after having read grid data from Pointwise, mesh has to be scaled (Pointwise works in millimeters, while Fluent in meters), checked and now all quantities of previous simulation was entered in the same way.
In order to execute two main simulations, the one at high subsonic and the other at low subsonic speed, two separate simulation settings and initializations were prepared. For the first one, a hybrid initialization was executed: max iteration number set at 500 for first order and 300 for third order (MUSCL), without using second order solver, which does not improve solution but only slows down the process. For the second one, only 75 iterations at first order and 75 iterations at the third are needed to reach convergence at 1e-5 residuals: this because at low subsonic speed the overall behaviour of the flow around the intake is simpler, no sonic transitions

take place around the cowl, and so less iterations are necessary for the same precision.

After the simulation run, two results file were exported by the software:
- a first file (.srp) contains information about drag coefficient, computed on the outer edge of the intake shape;
- a second file contains the average coefficient of pressure computed at mass flow inlet boundary;

This operation is repeated in the same way for both simulations. Now, Fluent process quit and post process will continue in MATLAB.

Post processing in MATLAB

The two file exported by Fluent are imported in MATLAB and their numerical data loaded in double variable. In this way, it possible to make the media between results at Mach = 0.84 and Mach = 0.3. The consequently data are put as value of fitness: while cd has to be minimized, cp has to be maximize, so, because by default the GA embedded performs a minimization, fitness become:fitness = [1/—cd— 1/cp].
Now the process ends and another simulation will take place.

3.3.3   The Optimization

In order to improve possibilities to reach Pareto Front, the optimization will be led with populations of at least three times the number of variables: in this case, 20 individuals look perfect. Also, the number of generation was set to 25. In this way, after 45 hours of computational time (estimated by a comparison between time of a single iteration and overall individuals run), process will end.
The embedded MATLAB function, for each iteration, will calculate new decisional variables, compare fitness results among individuals and, at the end, it will give the Pareto Front position, decisional variables of Pareto front individual, output messages and the complete last population computed data.
This function will start by, in order, reading first population variables, getting maximum number of generations, decisional variables and population dimension. It will also read boundary constraints of the variables (lower and upper). At the end, executes the fitness function, which is written in another script (see Appendix for the abstract of code).

3.4 Results

The optimization process data were memorized in one MATLAB data file, which contains information about individual, generation, decisional variables and fitness values. In Appendix, complete results of the optimization.
First thing to compute is the Pareto Front evolution: if after generations the front approaches at the utopia point, a sort of a limit for the process, the overall Pareto Front exists and is reached.
In fact, that's the point: results reach the target.
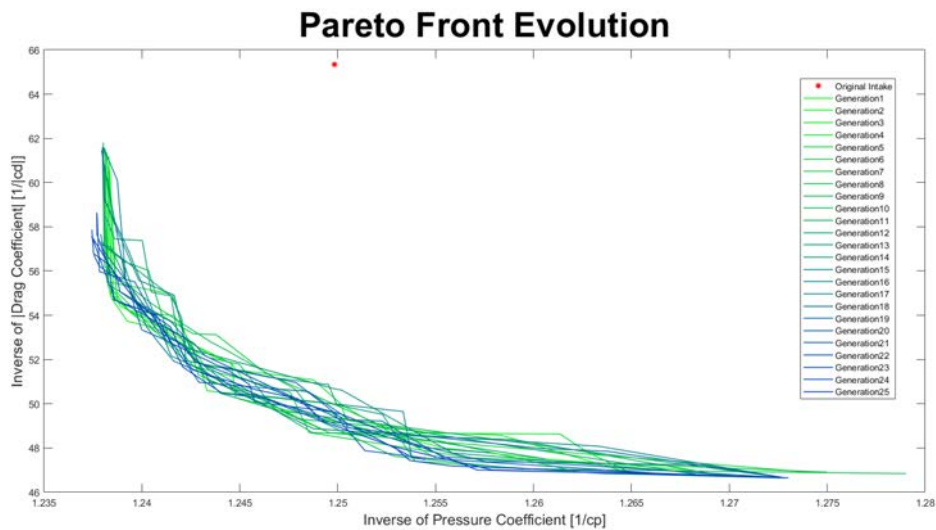
Figure 3.8: The evolution of Pareto front, compared with original intake data

It could be noticed that, generation by generation, the front advances in order to minimize target quantities, but variations are much closer to each other than expected: in fact, values of original intake are far away even from the first Pareto front, end generation by generation it is clear that the original shape has limited performance.
In fact, despite boundary constraints were entered as well as to prevent an excessive distortion, it is clear that new intakes have a completely new geometry.

After that, it was computed the overall Pareto Front of the process (Figure 3.9).
It could be seen that, throughout generations, the largest fitness distribution tends to reduce drag values much more than the increase of Cp. This fact is clearer by looking at Figure 3.10, in which new cowl geometries are plotted: the most representative cases are the one with the maximum coefficient of pressure, the one with minimum drag coefficient and another one in the middle, a media of both the extrema.
Figure 3.10 shows that the outer side of the intake changes in every condition, preferring a smoother curvature of the leading edge lip, according to the fact that the original intake has a cowl lip which was too sharp for drag efficiency.
Also, new intakes tend to have a smoother inner side. An interpretation of this phenomenon is given by the importance each run of each individual has in the
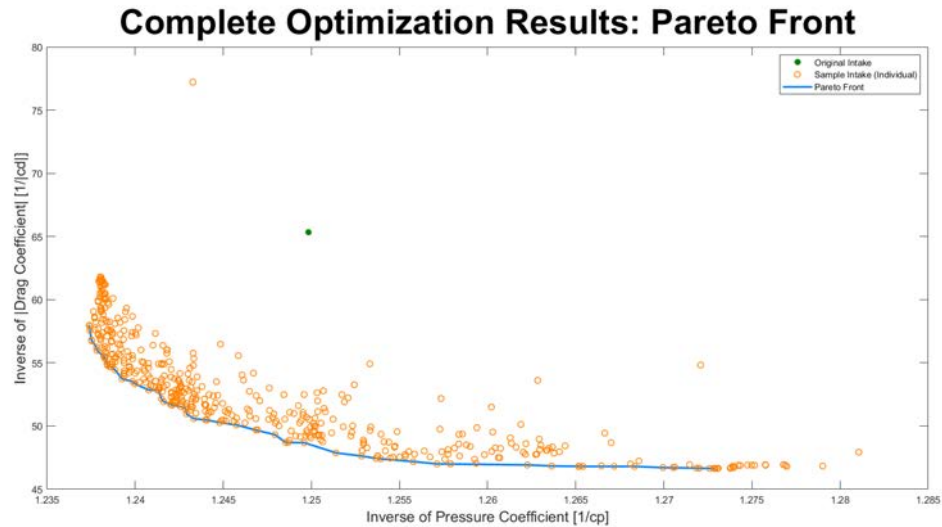
Figure 3.9: Pareto Front of the optimization process

global results: high subsonic speed, due to a greater compressibility of the air, get highest coefficient of pressure; this coefficient is increased if the intake accelerates less the flow, because there are fewer problems linked with higher Mach number flow induced by the thinner throat section (sonic transitions, fluid detachment); on the other hand, a smoother lip get to lower coefficient of drag at low subsonic flow, and so a lower global resistance.

Also, it could be seen that minimum drag intake has a shape closer to the original one, a sign that outer side influences, in these cases, the whole results much more than the inner one, and this fact is shown also by the shape of the Pareto Front, which main feature is to have better performance in drag reduction for every individual of which is composed.

These results tell exactly what the report by NASA explains.
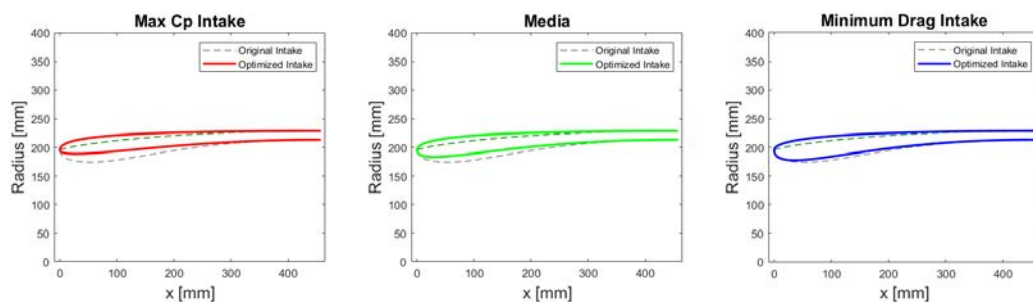
Figure 3.10: Three optimized intakes

At the end, this optimization lead to an important conclusion: NASA results in 1996 are really close to the final data of this process, and so the cowl lip influence in intake performance. This CFD model leads to same conclusions of wind tunnel tests, but now with an intake that, considering last results, could work better.

In order to understand better the behaviour of these two optimized intakes (max cp and min cd), a brief comparison among most important quantities.

Optimized Intake 1: Max Cp

In the previous pages, it was said that this intake would have worked at high subsonic fluxes instead a low speed, especially for what concerns fluid detachment caused by sharp cowl lip when Reynolds number is lower: in Figure 3.11 it is clear this fact.
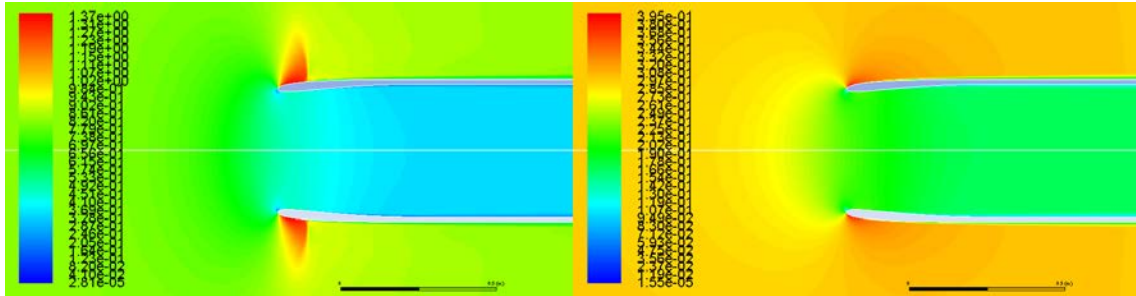
Figure 3.11: Comparison between max cp intake at 0.3 Mach and 0.84 Mach, contour of Mach number

It could be seen that there's no fluid detachment, especially at inner side, showing that pressure gradient is close to ideal solution for this kind of shape. Boundary layer thickness grows along the surfaces, but even with the contribution of sonic shocks at high speed, it never detaches externally. Also, a comparison between pressure coefficient inside the intake could precious for this post processing.
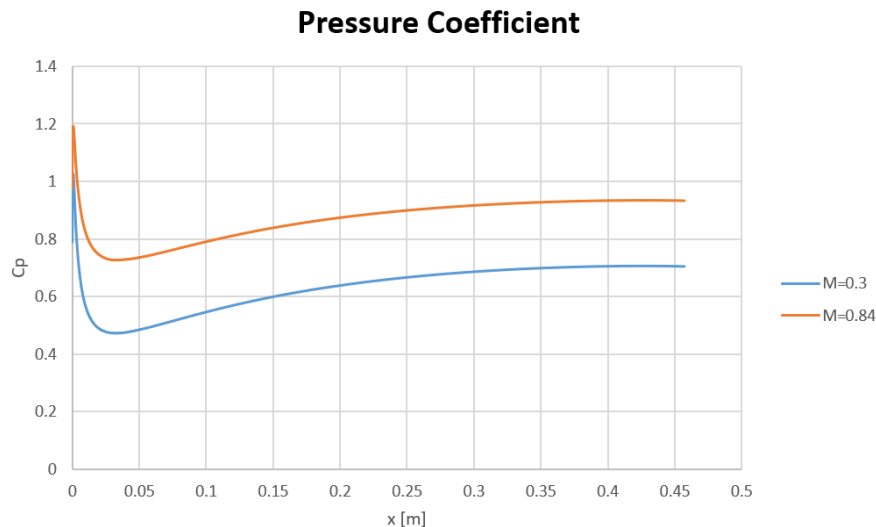
Figure 3.12: Comparison between max cp intake at 0.3 Mach and 0.84 Mach, plot of pressure coefficient at inner side

Pressure distribution is quite balanced between thinner section and mass flow inlet section, and so fluid gets a smoother compression inside the intake, whereas major contribution is given outside the cowl geometry, before air enters.

In fact, the increase in pressure recovery performance, despite the changes in the shape of the intake, are limited to 1%, whereas drag performance improves to 11.3% too.

Optimized Intake 1: Min Cd

For the other optimized intake, it could be expected that the airfoil at its inner side increases more air speed and so overall cp distribution is quite lower than in the other case.

For what concerns drag coefficient, the situation improves at its outer edge, whereas at the other side fluid detachment, especially at low Mach number, is caused by a greater variation of thickness, which cause higher pressure gradient along the surface (and that's why pressure coefficient is lower).
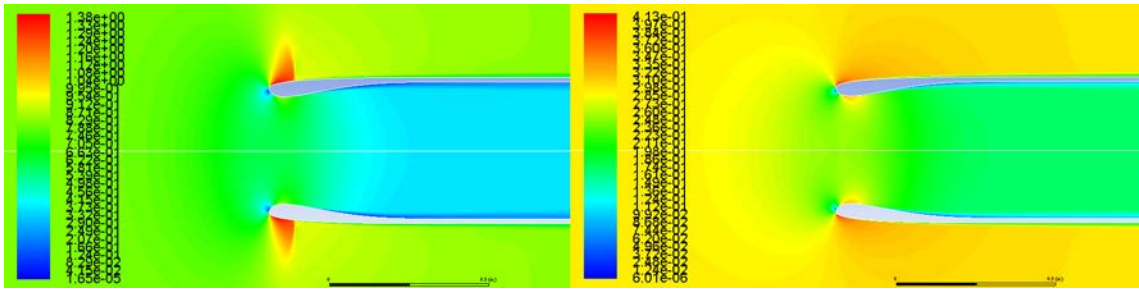
Figure 3.13: Comparison between min cd intake at 0.3 Mach and 0.84 Mach, contour of Mach number

From Figure 3.13, it is clear that the situation concerning pressure coefficient got worse, and this is exactly what a thicker airfoil does, increases air speed in its throat section much more than a thinner one.
The best evaluation of this optimized intake is given by numbers: instead a smooth worsening of pressure recovery (-1.85%), drag reduction reach the value of 28.62%.
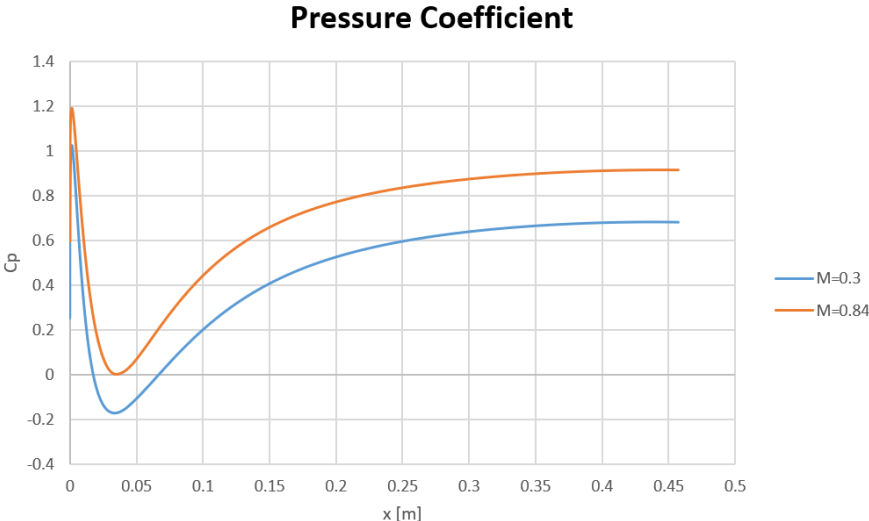
Figure 3.14: Comparison between min cd intake at 0.3 Mach and 0.84 Mach, plot of pressure coefficient at inner side

Chapter 4

Conclusions

In Figure 3.15, the two optimized intake geometries extruded by CAD software.
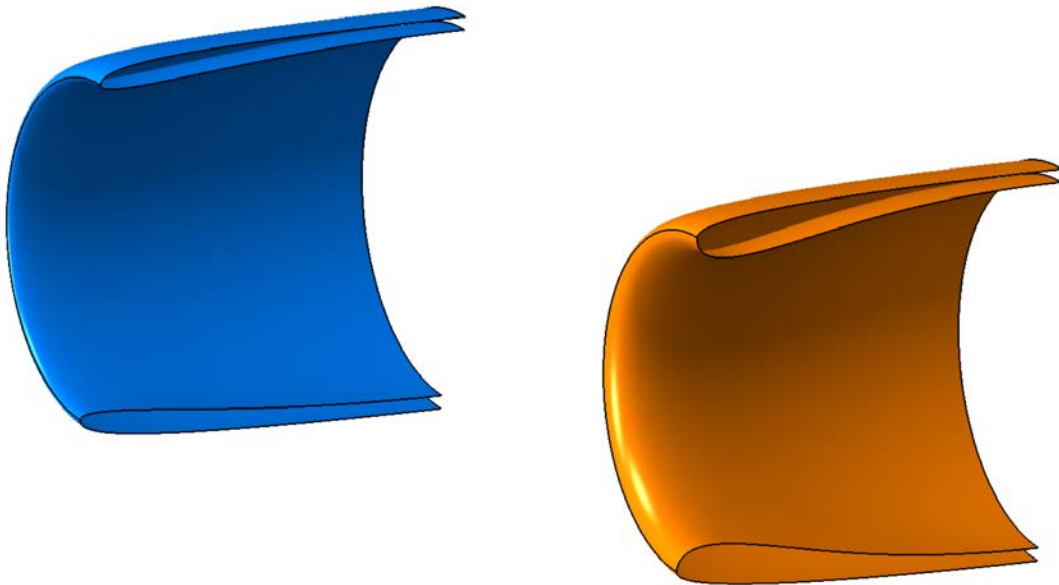
Figure 4.1: In blue, max cp intake; in orange, min cd intake

Optimization results confirm the importance of cowl lip shape in subsonic intake performance.

An important conclusion of the optimization process is the necessity of a smoother cowl lip, which now appears rounded between two sides for both the new airfoil shapes.

A sharp edge increases excessively the speed of the air in a small chord length, and so it is possible, for some particular geometries, to lead to a fluid detachment at outer side of the intake.

On the other hand, a sharper edge is particularly suitable for high subsonic / transonic intakes, because it limits sonic transitions at the inner edge, and also because it disperses better sonic shocks around the lip, reducing overall drag values at high speed.

Because of the decision to simulate airfoils at different range of speed, solution leads to a compromise shape for the new intake, allowing a reduction of thickness but also smoothing the lip of cowl leading edge.
Results explain that, both in case of search for maximum pressure recovery performance and minimum drag, a smoother lip is necessary for the purpose the intake was designed for, and so allowing the engine to make at best its work both at take off and on cruise.

For what concerns the CFD model, results proof that a smarter method for calculating and predicting intake performance and for a quicker simulation of its shape represents a good choice for an engineer.

With only 5 minutes needed to compute a complete run of simulation, and with data easy to compared to 1-dimension results, the model developed for this thesis reach its goal: increasing calculus capabilities and performance prediction of intakes without using a supercomputer, but only by a combination of MATLAB codes and good selection of meshing and solving software.

Computational Fluid Dynamics solves most of intakes questions, and the right way to employ these instruments will be pursued again years by years, with the hope, with this thesis, to be a part of this research.

Appendix

Wind Tunnel Tests

TABLE VI. Continued

(i) M = 0.84

mfr = 0.27 and α = 0°

φ = 0° Forebody X/L	CP	φ = 0° Afterbody X/L	CP	φ = 180° Forebody X/L	CP	φ = 180° Afterbody X/L	CP
-187.47	1.1500	343.16	-0.0368	-187.47	1.1525	343.16	-0.0291
-171.29	1.1513	384.14	-0.0358	-106.57	1.1381	384.14	-0.0362
-155.11	1.1503	419.13	-0.0368	-25.67	1.1116	419.13	-0.0345
-130.84	1.1470	457.12	-0.0305	-10.27	1.1779	457.12	-0.0352
-106.57	1.1395	507.77	-0.0238	-2.05	1.0637	507.77	-0.0285
-90.39	1.1294	545.76	-0.0105	0.00	-0.1979	545.76	-0.0171
-74.21	1.1222	571.08	0.0102	0.31	-1.1763	571.08	0.0082
-58.03	1.1101	583.74	0.0259	0.63	-1.4728	583.74	0.0283
-41.85	1.1032	596.41	0.0540	1.25	-1.5989	596.41	0.0543
-33.76	1.1064	609.07	0.1004	1.88	-1.6402	609.07	0.1074
-25.67	1.1112			2.50	-1.6487		
-23.11	1.1175			3.13	-1.6379		
-17.97	1.1348			3.75	-1.6203		
-10.27	1.1775			4.37	-1.5746		
-5.13	1.1811			5.00	-1.5637		
-3.34	1.1436			6.25	-1.5492		
-2.05	1.0644			7.50	-1.5172		
-0.90	0.8522			8.75	-1.4983		
-0.44	0.6400			10.00	-1.4639		
0.00	-0.3244			12.50	-1.4125		
0.31	-1.2279			15.00	-1.3778		
0.63	-1.4658			17.50	-1.3541		
1.25	-1.6083			20.00	-1.3242		
1.88	-1.6254			30.00	-1.2007		
2.50	-1.6326			50.00	-1.0174		
3.13	-1.6214			60.00	-0.9886		
3.75	-1.6057			70.00	-0.9412		
4.37	-1.5856			80.00	-0.9405		
5.00	-1.5701			90.00	-0.7423		
6.25	-1.5395			100.00	-0.4118		
7.50	-1.5000			110.00	-0.3686		
8.75	-1.4908			241.85	-0.0321		
10.00	-1.4582						
12.50	-1.4046						
15.00	-1.3926						
17.50	-1.3625						
20.00	-1.3194						
30.00	-1.1792						
40.00	-1.0763						
50.00	-1.0259						
60.00	-0.9676						
70.00	-0.9553						
80.00	-0.9317						
90.00	-0.7588						
100.00	-0.4208						
110.00	-0.3777						
241.85	-0.0406						
279.84	-0.0398						

mfr = 0.30 and α = 0°

φ = 0° Forebody X/L	CP	φ = 0° Afterbody X/L	CP	φ = 180° Forebody X/L	CP	φ = 180° Afterbody X/L	CP
-187.47	1.1436	343.16	-0.0341	-187.47	1.1430	343.16	-0.0234
-171.29	1.1439	384.14	-0.0321	-106.57	1.1260	384.14	-0.0308
-155.11	1.1417	419.13	-0.0308	-25.67	1.0868	419.13	-0.0204
-130.84	1.1344	457.12	-0.0241	-10.27	1.1637	457.12	-0.0291
-106.57	1.1249	507.77	-0.0104	-2.05	1.0927	507.77	-0.0164
-90.39	1.1170	545.76	0.0070	0.00	-0.1575	545.76	0.0020
-74.21	1.1052	571.08	0.0355	0.31	-1.1421	571.08	0.0308
-58.03	1.0934	583.74	0.0556	0.63	-1.4497	583.74	0.0606
-41.85	1.0819	596.41	0.0891	1.25	-1.5718	596.41	0.0914
-33.76	1.0794	609.07	0.1436	1.88	-1.6141	609.07	0.1467
-25.67	1.0846			2.50	-1.6278		
-23.11	1.0905			3.13	-1.6090		
-17.97	1.1112			3.75	-1.5907		
-10.27	1.1644			4.37	-1.5584		
-5.13	1.1859			5.00	-1.5381		
-3.34	1.1619			6.25	-1.5011		
-2.05	1.0913			7.50	-1.4769		
-0.90	0.8999			8.75	-1.4482		
-0.44	0.6916			10.00	-1.4172		
0.00	-0.2511			12.50	-1.3672		
0.31	-1.2388			15.00	-1.3501		
0.63	-1.4592			17.50	-1.3272		
1.25	-1.5751			20.00	-1.2849		
1.88	-1.5963			30.00	-1.1795		
2.50	-1.6068			50.00	-1.0257		
3.13	-1.5979			60.00	-0.9678		
3.75	-1.5748			70.00	-0.9545		
4.37	-1.5666			80.00	-0.9389		
5.00	-1.5338			90.00	-0.5028		
6.25	-1.5038			100.00	-0.3990		
7.50	-1.4790			110.00	-0.3307		
8.75	-1.4592			241.85	-0.0360		
10.00	-1.4338						
12.50	-1.3943						
15.00	-1.3542						
17.50	-1.3269						
20.00	-1.3058						
30.00	-1.1761						
40.00	-1.0783						
50.00	-1.0045						
60.00	-0.9639						
70.00	-0.9574						
80.00	-0.9256						
90.00	-0.4894						
100.00	-0.3748						
110.00	-0.3521						
241.85	-0.0418						
279.84	-0.0438						

mfr = 0.39 and α = 0°

φ = 0° Forebody X/L	CP	φ = 0° Afterbody X/L	CP	φ = 180° Forebody X/L	CP	φ = 180° Afterbody X/L	CP
-187.47	1.1073	343.16	-0.0244	-187.47	1.1045	343.16	-0.0133
-171.29	1.1064	384.14	-0.0197	-106.57	1.0772	384.14	-0.0170
-155.11	1.1034	419.13	-0.0103	-25.67	0.9806	419.13	-0.0063
-130.84	1.0939	457.12	0.0018	-10.27	1.0983	457.12	-0.0029
-106.57	1.0761	507.77	0.0276	-2.05	1.1574	507.77	0.0229
-90.39	1.0581	545.76	0.0641	0.00	0.1014	545.76	0.0594
-74.21	1.0381	571.08	0.1126	0.31	-0.9725	571.08	0.1049
-58.03	1.0131	583.74	0.1454	0.63	-1.3190	583.74	0.1438
-41.85	0.9934	596.41	0.1874	1.25	-1.4181	596.41	0.1891
-33.76	0.9825	609.07	0.2510	1.88	-1.4680	609.07	0.2547
-25.67	0.9821			2.50	-1.4922		
-23.11	0.9869			3.13	-1.4595		
-17.97	1.0128			3.75	-1.4451		
-10.27	1.0890			4.37	-1.4262		
-5.13	1.1758			5.00	-1.4043		
-3.34	1.1862			6.25	-1.3484		
-2.05	1.1568			7.50	-1.3379		
-0.90	1.0195			8.75	-1.2997		
-0.44	0.8566			10.00	-1.2703		
0.00	0.0408			12.50	-1.2214		
0.31	-1.0380			15.00	-1.2114		
0.63	-1.3154			17.50	-1.1858		
1.25	-1.4438			20.00	-1.1709		
1.88	-1.4590			30.00	-1.0715		
2.50	-1.4504			50.00	-0.9176		
3.13	-1.4576			60.00	-0.8972		
3.75	-1.4401			70.00	-0.8698		
4.37	-1.4240			80.00	-0.8620		
5.00	-1.3761			90.00	-0.3325		
6.25	-1.3616			100.00	-0.2509		
7.50	-1.3203			110.00	-0.1371		
8.75	-1.3084			241.85	-0.0362		
10.00	-1.2718						
12.50	-1.2421						
15.00	-1.2122						
17.50	-1.1833						
20.00	-1.1612						
30.00	-1.0545						
40.00	-0.9622						
50.00	-0.9281						
60.00	-0.8929						
70.00	-0.8705						
80.00	-0.8051						
90.00	-0.3352						
100.00	-0.2312						
110.00	-0.1403						
241.85	-0.0467						
279.84	-0.0374						

Figure 4.2: Wind tunnel data collection (for example, for Mach = 0.84)

NACA 1-85-100 with contraction ratio 1.250

M	mfr	α,deg	Table	Figure
Pressure coefficients				
0.79	0.61	0	VII(a)	10(a),12(a)
	.67	-2.0		11(a)
	↓	0		10(a),11(a),12(a)
		2.1		11(a)
	.74	0	↓	10(a),12(a)
0.84	0.49	-2.1	VII(b	11(b)
		-1.0		
		0		10(b),11(b),12(b),13(a)
		1.0		
		2.0		11(b),13(a)
		3.1		13(a)
	.55	0		
	.61	0		10(b),12(b)
	.67	-2.1		11(c)
		-1.0		
		0		10(b),11(c),12(b),13(b)
		1.0		
		2.0		11(c),13(b)
		3.1		13(b)
	.74	0		12(b)
	.83	-2.1		11(d)
	.83	-1.1		
	.84	0		10(b),11(d),12(b),13(c)
	.83	1.1		
		2.0		11(d),13(c)
		3.1	↓	13(c)
0.87	0.49	-2.0	VII(c)	11(e)
	↓	0		10(c),11(e),12(c),13(d)
		2.1		11(e),13(d)
	.55	0		
	.61			10(c),12(c)
	.67			10(c),12(c)
	.73	↓	↓	10(c),12(c)
0.89	0.49	-2.1	VII(d)	11(f)
	↓	0		10(d),11(f),12(d),13(e)
		2.0		11(f),13(e)
	.55	0		
	.61			10(d),12(d)
	.67			10(d),12(d)
	.73			12(d)
	.81	↓	↓	10(d),12(d)
0.92	0.49	0	VII(e)	10(e),12(e)
	.55			
	.61			10(e),12(e)
	.67			10(e),12(e)
	.73			12(e)
	.81	↓	↓	10(e),12(e)

Figure 4.3: Summary of wind tunnel tests conducted on the NACA 1-series

MATLAB codes

MATLAB script to compute main parameters of optimization and execute the overall process:

```
clearvars
close all

% clear results

global Ind Gen k results
Ind = 0;
Gen = 0;
k = 0;

%% Optimization parameters
nInd = 20;
nGen = 25;
nVar = 6;

% Bound constraints definition
% all sides
lb = [lb1 lb2 lb3 lb4 lb5];
ub = [ub1 ub2 ub3 ub4 ub5];


%% initialize the population
initPop = zeros(nInd,nVar);
for j=1:nInd
    initPop(j,:) = rand(1,(nVar)).*((ub-lb)+lb); %random
        intialization for first population
end
initPop(1,:) = [1 2 3 4 5 6];% first individual = original intake

results = zeros(1,10);

%% optimization

options=gaoptimset('PopulationSize',nInd,'InitialPopulation',
    initPop,'Generations',nGen);
[x,fval,exitflag,output,POPULATION,SCORE] = gamultiobj(@(decvar)
    fitnessFunction(decvar),nVar,[],[],[],[],lb,ub,options);
```

MATLAB function to execute airfoil creation and parametrization, mesh generation, fluent solver execution and post processing:

```matlab
function [fitness] = fitnessFunction(decvar)

global Ind Gen k results
Ind = Ind + 1;
k = k + 1;

dirOpt = strcat('opti_',num2str(Gen),'_',num2str(Ind),'\');
mkdir(dirOpt);
cd(dirOpt);

%% Plot Nacelle Airfoil
PB_in = [0 y1; 0 decvar(1); decvar(2) decvar(3); decvar(4) y4; x5
    y5];
PB_out = [0 y1_1; 0 decvar(5); decvar(6) y3_1; x4_1 y4_4];
t = 0:0.001:1;
B4 = bernsteinMatrix(4,t);
B3 = bernsteinMatrix(3,t);
bezierCurve_in = B4*PB_in;
bezierCurve_out = B3*PB_out;
x_in = bezierCurve_in(:,1);
r_in = bezierCurve_in(:,2);
x_out = bezierCurve_out(:,1);
r_out = bezierCurve_out(:,2);

%% Start up PW settings
fid = fopen('mesh.glf','w+');
fprintf(fid,'_____ ');
fprintf(fid,'_____ ');
%
%
% main instructions for PointWise
%
%
fclose(fid);

%% PW execution
system([pwd '\mesh.glf']);

%% Write Fluent journal
fid = fopen([pwd '\Journal_Fluent.jou'],'w+');
fprintf(fid,'%s%s%s\n',['file/read-case/ "',pwd,'\sim.cas"']);
%
%
% main instructions for Fluent
%
%
fclose(fid);

%% Run Fluent
system('"C:\.....\fluent.exe" 2ddp -g -t8 -i Journal_Fluent.jou');
```

```matlab
%% Read Report file
A = importdata('cp_084.srp');
cp_084 = A.data;
B = importdata('cd_084.frp');
cd_084 = B.data(1,4) + B.data(2,4);

C = importdata('cp_03.srp');
cp_03 = C.data;
D = importdata('cd_03.frp');
cd_03 = D.data(1,4) + D.data(2,4);

cP = (cp_084 + cp_03)/2;
cD = (cd_084 + cd_03)/2;

fitness = [1/cP cD];

results(k,:) = [Gen Ind decvar fitness];

cd ..
save results.mat results

if Ind == 20
    Ind = 0;
    Gen = Gen + 1;
end

end
```

Optimization Results
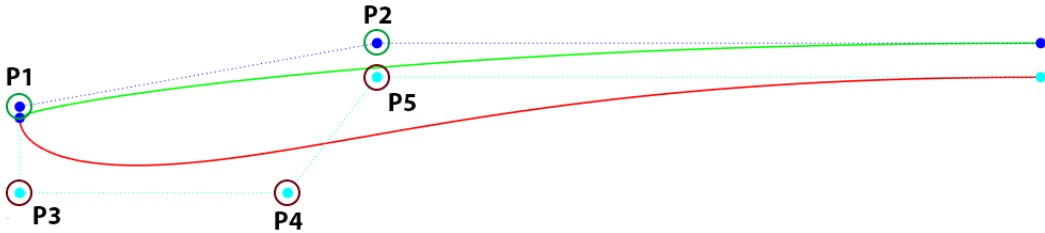
Figure 4.4: Bezier control point positions on airfoil shape

Gen	*Ind*	*y P1*	*x P2*	*y P3*	*x P4*	*y P4*	*x P5*	$\frac{1}{C_p}$	$\frac{1}{|C_d|}$
0	1	161.54	120.00	161.54	160.00	200.13	160.00	1.2498	65.3522
0	2	167.29	82.91	140.07	165.03	205.25	144.45	1.2602	51.5021
0	3	172.16	126.73	179.77	260.60	209.98	81.78	1.2416	53.1071
0	4	158.07	110.02	158.20	234.64	222.20	212.18	1.2644	48.4310
0	5	178.64	128.48	153.55	286.22	206.41	145.30	1.2467	54.1894
0	6	181.42	68.68	182.78	232.43	224.17	73.26	1.2381	61.4400
0	7	173.79	57.70	160.73	249.36	215.48	225.14	1.2446	51.8243
0	8	152.85	80.77	152.94	256.42	204.13	177.04	1.2721	54.8298
0	9	175.86	90.02	143.81	195.47	220.65	69.46	1.2524	53.2679
0	10	146.42	95.62	166.20	172.76	216.39	231.69	1.2555	47.9906
0	11	162.70	128.13	146.89	136.25	213.66	57.00	1.2667	49.4504
0	12	167.48	89.43	143.29	210.26	206.28	57.95	1.2670	48.6854
0	13	171.67	82.07	166.13	239.66	201.00	247.71	1.2433	77.2206
0	14	157.25	129.60	152.92	177.42	205.83	187.24	1.2628	53.6194
0	15	172.79	70.88	156.29	218.04	209.03	125.34	1.2490	50.9951
0	16	179.93	103.23	172.62	171.76	215.84	150.86	1.2394	54.1819
0	17	142.51	127.14	178.62	180.58	224.65	202.70	1.2607	47.4896
0	18	146.22	103.69	155.66	240.58	205.18	59.77	1.2681	46.9981
0	19	178.84	73.93	183.28	281.54	218.93	195.19	1.2386	54.8907
0	20	158.98	92.49	182.91	276.39	222.16	190.27	1.2448	50.2730
1	1	144.00	124.52	168.88	217.39	205.41	171.27	1.2574	52.1803
1	2	146.35	97.77	163.13	185.53	216.14	154.43	1.2651	46.8135
1	3	177.61	59.83	171.36	252.13	215.57	212.72	1.2412	53.5407
1	4	173.79	57.70	160.73	249.36	215.48	225.14	1.2446	51.8243
1	5	170.65	122.91	170.63	214.12	219.97	155.96	1.2435	52.2066
1	6	173.40	77.82	160.35	207.55	213.81	144.59	1.2451	51.1735
1	7	176.35	100.81	180.88	260.19	215.17	78.38	1.2394	55.0078
1	8	177.03	81.90	183.03	281.32	220.74	193.23	1.2389	54.4366

1	9	154.81	105.39	164.50	177.81	217.99	214.77	1.2584	48.5709
1	10	164.46	89.87	167.54	272.28	214.17	148.84	1.2505	50.2389
1	11	153.69	93.41	155.60	248.25	212.81	189.07	1.2544	48.7276
1	12	152.05	87.27	166.18	207.48	212.22	232.69	1.2619	50.1327
1	13	166.19	123.85	153.08	282.44	204.32	162.27	1.2533	54.9264
1	14	178.40	88.93	183.21	280.69	219.51	191.78	1.2387	54.8710
1	15	151.93	104.89	176.63	216.78	210.56	223.02	1.2493	51.6092
1	16	158.58	102.52	168.95	242.00	222.16	196.84	1.2505	49.3011
1	17	181.42	68.68	181.78	232.43	224.17	74.26	1.2383	61.1886
1	18	147.22	104.69	155.66	240.58	206.18	60.77	1.2747	46.9151
1	19	179.93	103.23	172.62	172.76	215.84	150.86	1.2394	54.1838
1	20	159.07	110.02	158.20	233.64	222.20	212.18	1.2622	48.6037
2	1	174.10	74.30	181.77	233.51	217.83	225.58	1.2393	53.7292
2	2	169.27	101.97	172.34	249.92	215.84	87.25	1.2433	52.2912
2	3	168.03	86.96	167.14	240.44	208.57	243.11	1.2459	55.5748
2	4	175.70	76.00	160.87	212.36	218.54	171.61	1.2440	51.6576
2	5	173.04	81.00	179.83	233.86	223.47	115.44	1.2408	54.9579
2	6	163.57	106.53	165.91	180.75	221.47	192.23	1.2502	49.9412
2	7	171.41	99.77	180.60	258.68	215.89	106.93	1.2414	53.1019
2	8	179.40	98.47	157.94	242.70	221.97	73.46	1.2448	56.4739
2	9	181.03	71.49	182.54	251.35	222.54	74.69	1.2383	60.0264
2	10	181.42	68.68	182.33	232.43	224.17	74.08	1.2382	61.2865
2	11	178.92	79.97	182.33	238.76	214.95	130.88	1.2384	54.8007
2	12	159.00	102.91	169.72	274.32	222.16	195.41	1.2511	49.4597
2	13	171.87	70.68	182.84	269.09	222.81	155.58	1.2406	53.4558
2	14	166.43	100.93	180.06	257.16	221.80	174.46	1.2429	51.8169
2	15	149.89	97.91	163.13	186.24	221.26	156.19	1.2550	47.5589
2	16	177.84	58.51	167.60	234.21	222.73	224.79	1.2423	52.6030
2	17	181.42	68.68	182.78	232.43	224.17	73.26	1.2381	61.4400
2	18	181.42	69.68	183.78	232.43	224.17	73.26	1.2380	61.6052
2	19	159.98	93.49	183.91	276.39	222.16	190.27	1.2433	50.5879
2	20	179.64	128.48	154.55	287.22	207.41	146.30	1.2461	54.0392
3	1	180.07	87.48	175.70	218.23	222.16	118.34	1.2392	56.1094
3	2	181.42	68.75	181.93	232.43	224.17	74.04	1.2382	61.2317
3	3	169.54	88.94	173.23	250.48	222.21	189.87	1.2432	51.7294
3	4	177.00	105.39	160.38	238.70	218.75	183.76	1.2444	52.3843
3	5	178.89	76.05	183.05	263.39	217.46	148.77	1.2384	54.9162
3	6	151.81	96.28	151.29	233.07	216.74	65.98	1.2811	47.9334
3	7	180.09	76.20	182.35	248.13	215.20	106.73	1.2383	55.3614
3	8	151.05	72.13	173.27	245.46	221.75	84.10	1.2573	49.7535
3	9	180.47	73.71	183.20	263.38	220.28	143.08	1.2383	55.8256
3	10	179.01	95.49	169.00	233.57	222.63	166.58	1.2417	53.9814
3	11	154.32	103.24	175.29	219.71	211.19	207.07	1.2488	51.0787
3	12	181.34	71.20	183.31	238.13	222.68	73.93	1.2381	60.4184

3	13	147.77	106.79	159.35	193.25	219.19	203.38	1.2715	46.9517
3	14	179.34	72.32	182.86	272.73	221.18	108.92	1.2386	56.6556
3	15	178.20	88.56	181.80	255.51	214.98	83.52	1.2388	55.3148
3	16	156.40	92.34	176.56	239.35	207.49	109.61	1.2502	50.0032
3	17	181.03	71.99	183.04	251.60	222.54	74.69	1.2383	60.1052
3	18	179.93	103.23	172.62	173.01	216.34	150.86	1.2394	54.1988
3	19	158.58	102.77	168.45	242.00	222.16	197.09	1.2504	49.2717
3	20	146.85	97.77	163.13	185.53	216.14	154.43	1.2623	46.9221
4	1	165.08	84.03	179.09	254.88	221.22	143.11	1.2433	51.5356
4	2	146.35	97.77	163.13	185.53	216.14	154.43	1.2651	46.8135
4	3	179.16	91.11	169.43	246.46	222.62	108.14	1.2418	55.7572
4	4	151.72	100.02	166.44	196.19	221.89	184.03	1.2628	47.7855
4	5	173.32	89.09	162.85	257.28	208.48	136.59	1.2447	52.4279
4	6	180.58	73.49	181.55	237.67	222.62	142.73	1.2384	56.1817
4	7	172.94	69.88	171.89	222.44	219.53	78.57	1.2430	54.1334
4	8	181.39	109.25	168.33	232.85	223.07	115.61	1.2410	56.3971
4	9	152.66	81.40	174.90	234.12	212.45	63.90	1.2496	48.6851
4	10	181.16	71.23	183.72	237.11	223.01	73.82	1.2381	60.6401
4	11	158.70	103.89	167.44	238.62	222.19	208.89	1.2499	49.2366
4	12	157.10	103.79	164.44	241.69	210.14	136.21	1.2540	49.3511
4	13	163.73	102.31	179.37	242.20	222.31	165.99	1.2429	51.3133
4	14	180.28	73.08	182.53	248.15	220.68	81.11	1.2384	58.2062
4	15	178.96	72.77	170.20	246.98	222.47	119.12	1.2415	54.9622
4	16	179.12	94.07	169.43	232.51	223.50	103.88	1.2416	56.3728
4	17	180.34	76.45	182.60	248.13	215.45	106.86	1.2383	55.5064
4	18	159.07	110.14	158.45	233.64	221.95	212.18	1.2614	48.6327
4	19	147.22	104.75	155.72	240.58	206.43	60.90	1.2752	46.8982
4	20	146.35	97.77	163.13	185.28	216.26	154.43	1.2652	46.8069
5	1	152.66	81.40	174.90	234.12	212.45	63.90	1.2496	48.6851
5	2	158.31	80.59	180.28	235.80	221.76	84.96	1.2471	51.9979
5	3	153.13	74.93	182.64	234.30	221.95	61.73	1.2496	52.4955
5	4	181.28	70.58	182.05	234.71	223.15	74.36	1.2383	60.4793
5	5	166.48	88.74	181.24	246.43	220.13	150.37	1.2423	51.8576
5	6	165.22	89.39	181.69	238.56	223.81	145.49	1.2426	52.2855
5	7	179.16	82.64	180.54	236.99	217.57	121.84	1.2387	55.0794
5	8	180.27	75.88	182.46	249.43	220.71	91.12	1.2385	57.6282
5	9	180.49	70.39	179.16	233.05	223.54	157.42	1.2386	55.6660
5	10	153.45	85.29	168.10	235.52	219.88	73.45	1.2594	49.8651
5	11	177.87	73.44	182.33	253.69	222.52	94.61	1.2387	57.3929
5	12	172.94	69.88	171.89	222.44	219.53	78.57	1.2430	54.1334
5	13	181.08	72.27	174.15	233.02	223.68	100.87	1.2394	57.5513
5	14	165.46	86.25	159.88	233.02	220.05	67.31	1.2521	52.2316
5	15	164.27	85.48	179.22	253.79	222.21	143.27	1.2429	51.5442
5	16	181.42	69.04	183.38	232.43	224.17	73.81	1.2381	61.4811

5	17	181.42	69.56	183.78	232.43	224.17	73.26	1.2380	61.6040
5	18	147.28	104.85	155.77	240.46	206.43	60.90	1.2758	46.9030
5	19	147.09	104.77	155.72	240.67	206.51	60.90	1.2742	46.8943
5	20	181.45	69.81	183.78	232.56	224.22	73.32	1.2381	61.6506
6	1	167.00	86.75	181.83	237.23	223.76	105.17	1.2425	54.1615
6	2	181.42	69.64	183.78	232.43	224.17	73.26	1.2380	61.6039
6	3	153.10	96.38	165.17	219.94	216.44	155.24	1.2641	47.9626
6	4	148.73	95.69	167.05	208.16	221.06	159.98	1.2567	47.5581
6	5	175.52	88.62	181.54	243.09	221.56	167.21	1.2394	54.1519
6	6	167.03	103.72	157.43	243.02	207.32	68.71	1.2523	50.0222
6	7	172.70	73.21	172.69	245.44	222.48	82.30	1.2433	55.3369
6	8	173.99	86.03	182.30	243.43	222.40	76.79	1.2398	57.4186
6	9	177.54	86.09	164.28	192.33	222.53	85.35	1.2433	55.7679
6	10	159.69	72.68	176.62	220.84	221.92	120.22	1.2476	50.5303
6	11	158.28	88.96	171.93	240.06	207.52	64.62	1.2504	49.2803
6	12	166.43	76.32	181.63	233.99	214.50	69.13	1.2420	52.3129
6	13	180.09	76.31	182.54	248.13	215.34	106.83	1.2383	55.4064
6	14	159.54	79.99	175.22	242.17	219.72	162.27	1.2489	49.6197
6	15	164.43	94.84	181.48	240.83	222.66	157.31	1.2426	51.7072
6	16	155.96	85.34	176.08	210.56	219.33	83.58	1.2494	50.4409
6	17	180.40	76.45	182.60	248.13	215.45	106.61	1.2382	55.5290
6	18	147.34	104.75	155.47	240.58	206.43	60.90	1.2750	46.9073
6	19	152.85	81.40	174.90	234.37	212.20	64.02	1.2485	48.6974
6	20	181.42	69.56	183.78	232.43	224.42	73.26	1.2380	61.7913
7	1	147.82	96.82	165.52	229.13	215.69	146.56	1.2539	47.4020
7	2	149.39	94.20	172.89	214.13	220.87	118.40	1.2616	48.3195
7	3	181.42	69.67	183.78	232.43	224.17	73.26	1.2380	61.6053
7	4	176.43	70.68	181.18	229.33	223.58	77.34	1.2390	58.5539
7	5	157.68	91.76	181.29	204.14	223.31	113.50	1.2464	51.3526
7	6	155.72	86.98	155.84	234.96	212.31	69.59	1.2564	48.0268
7	7	149.80	89.71	165.87	249.64	215.09	72.17	1.2578	48.1320
7	8	155.86	97.61	163.22	193.92	219.00	119.05	1.2588	48.5168
7	9	179.40	88.28	178.53	233.25	223.13	152.08	1.2389	55.4727
7	10	170.34	80.17	175.89	233.20	216.09	70.93	1.2426	53.1658
7	11	160.78	71.51	182.30	231.16	223.01	86.14	1.2438	53.1228
7	12	149.46	100.28	157.05	245.75	213.50	97.80	1.2743	46.8808
7	13	181.32	71.73	183.33	232.71	223.77	74.02	1.2381	61.1566
7	14	159.88	85.43	161.02	233.73	206.95	62.96	1.2530	48.7157
7	15	146.60	102.08	160.88	190.23	211.17	77.24	1.2720	46.6655
7	16	180.81	72.21	182.71	249.48	216.42	96.10	1.2382	56.0875
7	17	146.35	97.77	163.63	185.28	216.51	154.43	1.2636	46.8377
7	18	146.35	97.77	163.13	185.78	216.26	154.93	1.2654	46.8103
7	19	181.03	71.99	183.29	251.60	223.04	74.69	1.2382	60.4709
7	20	179.59	76.81	182.79	248.13	215.84	107.08	1.2383	55.3746

8	1	150.43	90.80	173.27	239.01	220.55	87.63	1.2586	49.3612
8	2	181.09	71.79	183.02	239.24	223.27	81.13	1.2382	60.0301
8	3	180.43	74.41	183.00	237.55	224.00	92.28	1.2383	59.3480
8	4	181.42	70.13	183.69	232.56	223.92	73.74	1.2380	61.3656
8	5	171.47	75.44	182.38	235.39	217.69	73.16	1.2405	54.5281
8	6	177.86	90.04	159.09	247.11	215.12	100.86	1.2442	52.4840
8	7	163.14	90.70	171.70	242.54	217.54	100.96	1.2478	50.6761
8	8	146.85	103.23	159.40	238.40	211.98	65.52	1.2790	46.8406
8	9	181.25	71.80	182.92	233.14	223.44	74.27	1.2381	60.8144
8	10	149.74	89.74	163.68	248.29	214.72	91.55	1.2528	47.6308
8	11	176.51	71.00	181.92	228.42	222.14	73.85	1.2389	58.0995
8	12	160.82	83.19	183.38	210.17	224.11	74.47	1.2433	54.7873
8	13	181.42	69.67	183.78	232.43	224.17	73.26	1.2380	61.6052
8	14	162.25	90.66	181.37	225.16	223.67	107.92	1.2435	52.8015
8	15	156.47	80.92	175.60	223.91	215.27	102.20	1.2491	49.2128
8	16	181.19	71.73	182.88	233.85	221.54	94.00	1.2381	58.1785
8	17	181.42	69.67	183.78	233.43	224.17	73.26	1.2380	61.6041
8	18	147.35	98.77	163.13	186.78	216.26	154.93	1.2593	47.0565
8	19	180.81	71.21	183.71	249.48	216.42	96.10	1.2381	56.2005
8	20	181.42	69.68	183.78	231.43	224.17	73.26	1.2380	61.6048
9	1	172.62	100.11	178.42	244.17	212.39	90.18	1.2414	52.9694
9	2	181.32	70.95	183.24	233.38	223.47	82.05	1.2380	60.1841
9	3	174.56	72.06	168.90	237.78	214.22	64.69	1.2432	53.0710
9	4	156.30	98.86	163.31	236.15	212.81	91.91	1.2590	48.3794
9	5	178.00	71.89	178.39	225.07	221.68	96.37	1.2391	56.4133
9	6	180.81	70.81	183.69	241.91	217.17	78.08	1.2381	57.1263
9	7	160.08	78.44	179.77	215.79	222.73	104.05	1.2450	51.7893
9	8	174.47	96.08	178.66	219.08	220.42	80.07	1.2403	56.0260
9	9	181.09	71.74	182.94	236.74	222.37	85.47	1.2381	59.1321
9	10	156.71	71.38	170.07	230.95	218.79	72.15	1.2493	50.2568
9	11	160.54	78.67	180.72	235.27	221.43	66.92	1.2446	53.5161
9	12	160.71	71.97	182.74	222.56	222.06	99.96	1.2434	52.0834
9	13	160.61	90.38	174.66	242.90	206.71	94.27	1.2480	50.3932
9	14	159.64	79.17	176.45	205.15	212.55	97.20	1.2469	49.6809
9	15	157.32	90.23	179.89	217.52	217.34	64.63	1.2476	51.2366
9	16	152.33	92.76	164.14	238.73	216.79	80.95	1.2630	48.4777
9	17	181.42	69.93	184.03	230.93	224.42	73.51	1.2380	61.8093
9	18	152.85	81.90	174.90	234.37	212.20	64.02	1.2487	48.7025
9	19	181.42	70.13	183.19	232.56	224.17	73.74	1.2382	61.4756
9	20	146.60	102.58	161.38	190.23	211.17	77.24	1.2699	46.7121
10	1	173.90	72.13	176.74	231.73	221.88	98.18	1.2413	54.9292
10	2	174.07	73.75	177.96	229.43	217.10	95.54	1.2405	53.7184
10	3	173.85	98.77	171.77	242.52	213.66	80.92	1.2429	52.9606
10	4	169.34	72.67	177.14	228.18	216.81	78.67	1.2424	52.8443

10	5	179.27	71.75	182.05	226.69	223.45	76.13	1.2384	59.7589
10	6	176.42	84.37	178.52	239.48	217.12	91.08	1.2397	54.7159
10	7	181.42	69.68	183.78	233.13	224.17	73.26	1.2380	61.6050
10	8	181.42	69.68	183.78	231.43	224.17	73.26	1.2380	61.6048
10	9	162.45	82.83	177.51	230.93	215.33	112.62	1.2440	50.4841
10	10	167.43	98.56	172.54	197.33	213.22	95.41	1.2431	51.2754
10	11	180.81	70.81	183.69	241.91	217.17	78.08	1.2381	57.1263
10	12	180.94	70.29	183.72	239.18	221.06	77.36	1.2381	59.0401
10	13	178.03	71.95	171.96	231.84	222.00	72.38	1.2411	57.3268
10	14	163.49	101.45	168.30	225.30	218.60	92.39	1.2495	51.0769
10	15	177.87	88.85	179.50	232.82	222.72	81.95	1.2391	58.1985
10	16	174.15	77.21	181.58	235.66	221.24	70.04	1.2398	57.1295
10	17	178.18	72.07	178.64	225.07	221.68	96.49	1.2390	56.4970
10	18	159.83	79.17	176.20	205.15	212.55	97.20	1.2469	49.6980
10	19	181.32	70.95	183.30	233.13	223.47	82.05	1.2380	60.1928
10	20	146.60	102.08	160.63	190.23	211.17	77.24	1.2728	46.6501
11	1	181.26	69.94	183.77	232.05	223.94	76.95	1.2381	61.0107
11	2	180.46	71.68	183.70	234.59	224.09	88.50	1.2382	59.7783
11	3	181.25	70.92	183.69	234.06	217.28	78.20	1.2379	57.3160
11	4	171.30	85.32	172.49	211.90	211.98	78.35	1.2427	52.0208
11	5	150.89	71.28	161.08	238.09	219.58	71.21	1.2529	48.8900
11	6	173.99	91.15	163.50	198.33	219.08	74.49	1.2435	53.9056
11	7	168.18	71.54	182.07	240.67	221.30	109.44	1.2418	53.2538
11	8	181.36	69.69	183.42	231.63	223.63	80.11	1.2380	60.4922
11	9	173.89	97.45	171.84	237.23	219.01	78.94	1.2431	54.6018
11	10	154.11	70.62	182.56	218.10	213.78	75.77	1.2479	49.3165
11	11	150.96	74.09	177.09	235.11	223.22	86.94	1.2512	50.5458
11	12	172.24	71.96	177.81	227.08	221.86	92.21	1.2415	54.8741
11	13	177.04	93.76	179.15	228.86	223.86	73.85	1.2395	59.3238
11	14	175.84	71.41	169.88	235.66	214.72	65.56	1.2425	53.6127
11	15	173.85	98.77	171.77	242.52	213.66	80.92	1.2429	52.9606
11	16	178.90	71.69	176.70	231.71	223.32	73.06	1.2395	59.0423
11	17	147.10	102.08	161.13	190.73	211.67	77.24	1.2683	46.8038
11	18	147.35	103.48	159.40	238.90	212.48	65.77	1.2768	46.9517
11	19	147.35	103.48	159.40	238.65	211.98	65.77	1.2769	46.8959
11	20	180.81	70.81	184.19	241.91	217.67	78.08	1.2381	57.3944
12	1	150.91	73.04	176.11	237.24	220.47	85.70	1.2523	49.5168
12	2	170.45	81.07	175.92	210.42	212.48	88.50	1.2423	52.0327
12	3	178.96	70.73	182.01	233.97	222.92	72.37	1.2385	59.6181
12	4	168.78	73.51	175.85	219.90	213.75	75.32	1.2423	51.9524
12	5	162.87	77.79	164.52	191.21	215.50	77.82	1.2500	49.9486
12	6	163.52	69.82	171.91	231.99	221.86	73.11	1.2476	53.0081
12	7	178.42	74.46	172.54	222.45	217.01	75.15	1.2405	55.0524
12	8	162.55	77.90	170.28	237.80	217.26	76.61	1.2495	50.8679

12	9	147.46	91.03	171.47	223.38	212.07	81.25	1.2606	47.5047
12	10	172.24	71.96	177.81	227.08	221.86	92.21	1.2415	54.8741
12	11	171.30	85.32	172.49	211.90	211.98	78.35	1.2427	52.0208
12	12	160.30	72.68	176.67	223.06	221.22	98.56	1.2465	51.2027
12	13	166.94	89.60	177.02	235.56	217.04	72.32	1.2430	52.8093
12	14	180.54	70.95	182.70	230.40	221.14	82.49	1.2382	58.4411
12	15	178.11	71.68	182.16	236.08	222.34	92.83	1.2386	57.4527
12	16	177.06	81.82	176.04	215.40	222.25	78.24	1.2400	57.3811
12	17	176.84	71.41	169.88	236.66	214.72	65.56	1.2420	53.8765
12	18	150.43	91.80	173.27	239.01	220.55	88.63	1.2584	49.3397
12	19	151.43	90.80	173.27	240.01	220.55	88.63	1.2549	49.5569
12	20	150.89	71.28	161.08	238.09	218.58	71.21	1.2530	48.5715
13	1	156.37	86.56	176.31	239.16	221.02	95.88	1.2502	50.6153
13	2	179.79	81.21	183.26	234.52	222.92	73.34	1.2383	60.1498
13	3	179.64	73.02	181.77	228.41	218.69	78.67	1.2384	57.0918
13	4	181.26	70.50	183.73	233.10	223.58	73.46	1.2380	61.0965
13	5	177.76	71.10	181.85	236.18	220.79	81.34	1.2387	57.2507
13	6	181.42	69.68	183.78	231.43	224.17	73.26	1.2380	61.6048
13	7	168.09	87.85	161.96	234.91	220.24	75.12	1.2503	52.6337
13	8	171.92	71.51	174.19	212.28	214.42	77.82	1.2421	52.5826
13	9	157.03	84.27	173.07	229.66	219.30	77.36	1.2497	50.6970
13	10	179.79	71.08	182.68	237.87	224.08	102.48	1.2383	58.3552
13	11	175.33	94.42	171.28	225.63	213.96	68.32	1.2424	53.6222
13	12	150.42	89.21	163.81	203.58	213.97	75.39	1.2558	47.7786
13	13	181.27	73.92	178.38	226.93	219.51	78.43	1.2386	57.5967
13	14	176.08	71.53	177.22	227.02	215.10	78.13	1.2400	54.1744
13	15	177.12	71.36	177.57	236.02	214.95	73.48	1.2397	54.6379
13	16	178.66	71.54	174.37	235.92	221.72	71.50	1.2402	57.7742
13	17	181.25	71.42	184.19	234.31	216.78	78.20	1.2379	57.1975
13	18	178.67	74.46	172.54	222.45	217.01	75.65	1.2404	55.0990
13	19	146.85	102.58	160.88	190.73	211.17	77.74	1.2705	46.7177
13	20	147.10	101.58	160.63	190.23	211.67	77.24	1.2706	46.7503
14	1	170.70	71.44	179.86	238.83	220.55	77.86	1.2416	54.9062
14	2	169.37	72.47	175.59	233.81	214.77	74.95	1.2423	52.2887
14	3	158.93	78.43	177.47	233.20	222.82	81.59	1.2484	52.4818
14	4	153.40	87.42	164.04	227.07	216.29	91.41	1.2630	48.1555
14	5	169.65	74.94	163.27	234.08	218.94	75.46	1.2469	52.4023
14	6	151.42	88.99	174.27	239.09	220.94	90.86	1.2533	49.6500
14	7	172.86	71.52	182.18	238.75	221.29	87.43	1.2398	55.5857
14	8	179.31	72.63	180.44	230.80	220.72	71.74	1.2385	58.2563
14	9	157.79	82.30	181.14	240.52	221.14	109.29	1.2465	50.7877
14	10	146.93	88.74	168.92	237.96	219.81	80.25	1.2541	48.7589
14	11	180.69	70.65	182.86	231.03	221.98	78.22	1.2381	59.2883
14	12	162.94	81.44	174.68	221.98	213.11	78.34	1.2450	50.4681

14	13	165.39	70.82	163.25	234.83	221.67	74.13	1.2517	52.4820
14	14	150.42	89.38	164.13	219.21	214.82	87.28	1.2553	47.7569
14	15	164.59	69.81	172.10	231.82	222.55	73.20	1.2461	53.6408
14	16	167.42	78.20	178.94	239.85	221.08	101.29	1.2426	53.0948
14	17	181.42	69.68	183.78	230.43	224.17	73.26	1.2380	61.6053
14	18	164.52	69.82	171.91	232.99	220.86	74.11	1.2465	52.7504
14	19	157.37	87.56	176.31	239.16	220.02	95.88	1.2499	50.5291
14	20	149.42	90.21	163.81	203.58	213.97	75.39	1.2538	47.6456
15	1	175.49	70.27	181.72	227.99	221.45	74.54	1.2391	57.2628
15	2	155.60	87.44	170.41	210.84	213.32	77.48	1.2488	48.8746
15	3	162.81	83.22	174.91	229.05	214.32	92.88	1.2449	50.4367
15	4	174.89	84.89	182.44	237.41	221.36	80.89	1.2393	56.8595
15	5	181.42	69.68	183.78	231.10	224.17	73.26	1.2380	61.6048
15	6	157.46	75.25	159.51	236.74	212.99	67.95	1.2635	48.2384
15	7	169.06	73.38	181.23	233.94	211.62	77.36	1.2415	52.1603
15	8	147.41	73.08	173.08	238.02	221.08	81.08	1.2613	49.0701
15	9	146.85	103.23	159.40	238.40	211.98	65.52	1.2790	46.8406
15	10	146.60	102.08	160.63	190.23	211.17	77.24	1.2728	46.6501
15	11	167.45	70.34	177.05	232.12	217.05	73.19	1.2428	52.6391
15	12	147.45	91.85	172.91	208.82	219.92	79.98	1.2629	48.9660
15	13	181.40	70.53	183.72	234.04	220.70	73.31	1.2380	59.3188
15	14	169.12	92.54	170.80	226.02	211.60	75.06	1.2432	51.4932
15	15	165.34	77.79	181.57	228.19	218.14	73.60	1.2425	52.9992
15	16	156.34	86.61	167.21	235.21	212.69	71.70	1.2506	48.7608
15	17	153.40	87.42	164.04	227.07	215.79	91.41	1.2633	48.0790
15	18	147.35	103.48	159.65	238.90	212.23	65.77	1.2758	46.9394
15	19	151.92	89.24	174.52	239.09	221.44	91.11	1.2518	49.9425
15	20	162.94	81.94	174.68	221.98	212.61	78.84	1.2452	50.3984
16	1	172.43	73.65	180.15	230.28	217.28	73.60	1.2405	54.3579
16	2	175.18	78.96	182.45	235.05	218.18	79.37	1.2392	55.5584
16	3	146.91	103.13	163.76	231.37	213.62	69.08	1.2593	47.3717
16	4	164.34	85.65	174.61	231.13	215.54	84.98	1.2443	51.1101
16	5	164.84	80.49	173.49	233.11	215.79	89.99	1.2441	50.9987
16	6	181.42	69.68	183.78	231.31	224.17	73.26	1.2380	61.6054
16	7	155.53	101.01	177.12	233.06	222.93	71.45	1.2507	52.7850
16	8	148.45	87.04	161.56	191.12	217.38	76.62	1.2598	47.7328
16	9	149.72	99.97	169.81	201.25	211.41	76.53	1.2627	47.7459
16	10	146.62	102.72	160.42	190.81	211.68	67.52	1.2740	46.7475
16	11	146.60	102.08	160.63	190.23	211.17	77.24	1.2728	46.6501
16	12	149.20	95.19	160.82	221.32	212.79	66.35	1.2576	47.3820
16	13	172.35	73.13	179.59	235.39	211.96	76.56	1.2408	52.8509
16	14	154.41	89.43	170.85	220.91	215.48	77.21	1.2500	49.0570
16	15	180.09	70.96	179.26	234.53	223.65	72.82	1.2387	60.0955
16	16	170.25	71.64	183.34	234.03	215.83	77.45	1.2403	53.4625

16	17	168.06	73.38	181.23	233.94	211.62	77.36	1.2416	51.9298
16	18	147.85	104.23	160.40	238.40	212.98	64.52	1.2686	47.2291
16	19	178.66	71.54	174.37	235.92	220.72	71.50	1.2401	57.2047
16	20	173.86	71.52	182.18	238.75	221.29	87.43	1.2396	55.9003
17	1	152.15	91.92	169.93	218.21	213.89	77.24	1.2581	48.2519
17	2	177.12	71.36	177.57	236.02	214.95	73.48	1.2397	54.6379
17	3	174.27	71.35	170.21	201.44	216.01	71.40	1.2426	53.3749
17	4	175.47	78.55	178.20	235.34	215.21	74.09	1.2401	54.3662
17	5	150.61	86.26	168.79	210.64	214.19	75.25	1.2620	47.9345
17	6	162.62	78.90	177.15	232.25	215.83	81.69	1.2435	51.0181
17	7	181.28	70.30	183.75	232.93	224.12	73.57	1.2381	61.4877
17	8	149.76	86.43	163.57	194.75	216.87	79.60	1.2542	48.0328
17	9	173.15	85.50	176.70	229.21	215.50	75.01	1.2415	53.7016
17	10	161.70	100.79	170.74	224.64	219.40	71.78	1.2504	51.9913
17	11	176.60	92.57	170.83	230.18	216.03	69.59	1.2420	54.4879
17	12	181.42	69.68	183.78	231.43	224.17	73.26	1.2380	61.6048
17	13	169.51	100.17	167.94	215.08	213.48	75.60	1.2440	51.6821
17	14	175.18	78.96	182.45	235.05	218.18	79.37	1.2392	55.5584
17	15	168.32	78.00	179.49	232.70	216.62	77.82	1.2423	52.8661
17	16	163.51	76.54	176.25	232.20	218.23	72.14	1.2439	52.1371
17	17	148.45	87.04	162.06	191.37	217.38	77.12	1.2578	47.7828
17	18	181.92	69.93	184.03	231.35	223.67	73.51	1.2379	61.4591
17	19	181.42	69.68	183.28	231.43	224.17	73.26	1.2381	61.5303
17	20	164.34	86.15	174.61	231.38	215.79	85.23	1.2442	51.1622
18	1	158.75	93.25	170.75	222.56	219.25	73.53	1.2508	51.1424
18	2	180.49	70.95	183.13	234.37	221.03	77.06	1.2382	58.8042
18	3	152.42	83.27	160.09	198.06	212.01	70.36	1.2553	47.6002
18	4	157.22	100.31	164.20	197.81	215.23	74.30	1.2522	49.2200
18	5	181.79	72.43	180.23	231.73	218.16	75.80	1.2384	57.5479
18	6	155.79	89.68	159.77	203.91	212.03	67.76	1.2634	48.0795
18	7	181.83	70.01	183.94	233.06	221.27	73.38	1.2379	59.8364
18	8	162.36	82.01	175.58	226.99	216.09	76.75	1.2452	51.0434
18	9	146.60	102.08	160.63	190.23	211.17	77.24	1.2728	46.6501
18	10	164.13	79.35	175.02	232.78	215.79	81.82	1.2440	51.1573
18	11	152.79	103.06	161.49	231.96	213.09	67.76	1.2607	48.2301
18	12	162.24	94.02	178.94	209.58	213.74	77.31	1.2429	50.9707
18	13	153.14	71.90	183.23	203.87	219.28	75.14	1.2485	50.5540
18	14	146.61	102.49	160.49	190.76	211.48	69.85	1.2739	46.7051
18	15	169.76	73.84	180.39	236.27	213.53	68.87	1.2415	52.7414
18	16	175.07	75.17	181.82	231.96	223.91	77.49	1.2394	58.4179
18	17	182.25	71.92	183.69	234.06	217.28	78.20	1.2379	57.6762
18	18	154.41	89.43	170.85	221.91	216.48	77.21	1.2506	49.2709
18	19	179.66	72.54	174.37	236.92	222.72	72.50	1.2398	58.6758
18	20	180.25	71.92	183.69	234.06	217.28	79.20	1.2380	56.9370

19	1	153.96	91.14	170.70	215.11	215.18	77.21	1.2505	48.9083
19	2	146.61	102.41	160.55	190.81	211.40	75.77	1.2738	46.6695
19	3	169.94	95.04	161.52	209.02	212.60	74.13	1.2479	50.9539
19	4	146.75	102.23	160.27	237.71	211.96	68.30	1.2770	46.8037
19	5	173.34	73.67	176.39	236.07	220.91	69.62	1.2418	56.0176
19	6	172.03	77.08	182.58	192.78	219.32	71.50	1.2396	55.5073
19	7	148.78	101.52	168.68	217.81	214.52	77.21	1.2602	47.9907
19	8	151.80	92.07	166.52	225.39	215.41	73.78	1.2637	48.3519
19	9	146.60	102.08	160.63	190.23	211.17	77.24	1.2728	46.6501
19	10	163.80	90.25	175.00	203.05	216.87	75.29	1.2439	51.7012
19	11	152.05	83.41	166.08	234.74	212.27	68.98	1.2638	47.8520
19	12	180.44	73.58	183.09	192.18	214.07	77.47	1.2378	55.9769
19	13	146.61	102.25	160.49	190.31	211.43	68.64	1.2738	46.7137
19	14	176.60	92.57	170.83	230.18	216.03	69.59	1.2420	54.4879
19	15	181.42	69.68	183.78	231.10	224.17	73.26	1.2380	61.6048
19	16	176.35	101.06	164.04	191.74	215.65	74.39	1.2432	53.4920
19	17	146.62	101.72	160.42	190.81	212.68	67.52	1.2739	46.8285
19	18	169.76	72.84	181.39	237.27	213.53	68.87	1.2413	52.8332
19	19	183.25	71.92	184.69	235.06	218.28	79.20	1.2377	58.5406
19	20	154.41	90.43	170.85	220.91	216.48	78.21	1.2503	49.2618
20	1	159.55	86.44	169.50	231.39	219.78	71.82	1.2507	51.3985
20	2	181.03	72.62	183.51	219.73	214.29	77.90	1.2378	56.2432
20	3	147.30	79.30	181.66	205.47	211.61	78.06	1.2514	47.8788
20	4	172.03	77.08	182.58	192.78	219.32	71.50	1.2396	55.5073
20	5	171.93	94.20	182.19	210.84	212.82	77.62	1.2400	53.3423
20	6	146.61	102.17	160.60	190.75	211.21	76.44	1.2730	46.6520
20	7	170.45	74.84	163.17	217.51	211.60	70.70	1.2455	50.8588
20	8	178.89	85.75	175.44	200.98	215.08	70.51	1.2394	55.2222
20	9	181.44	72.21	183.70	193.45	215.47	78.62	1.2375	56.7412
20	10	161.10	74.38	168.14	190.72	213.87	72.64	1.2497	49.6378
20	11	165.04	78.42	172.20	229.67	216.46	74.77	1.2445	51.4681
20	12	151.59	90.91	160.41	191.72	211.62	75.00	1.2546	47.5334
20	13	168.32	78.00	179.49	232.70	216.62	77.82	1.2423	52.8661
20	14	159.03	96.66	178.91	191.50	212.01	75.15	1.2457	50.0857
20	15	170.99	72.67	181.32	233.32	217.10	79.05	1.2408	53.7937
20	16	179.04	90.20	173.17	190.95	212.69	76.03	1.2397	54.2395
20	17	169.76	72.84	181.39	237.27	213.53	69.87	1.2413	52.8065
20	18	169.76	73.84	181.39	237.27	213.53	68.87	1.2413	52.8422
20	19	182.25	71.92	184.69	233.06	218.28	78.20	1.2378	58.2328
20	20	147.60	103.08	160.63	190.23	211.17	77.24	1.2665	46.8485
21	1	150.72	98.62	160.10	194.27	211.62	75.37	1.2545	47.4679
21	2	154.65	94.45	164.93	212.09	218.46	72.99	1.2603	49.5279
21	3	151.64	95.15	162.42	216.93	214.08	78.15	1.2574	47.9679
21	4	177.33	78.09	176.71	230.65	217.23	76.17	1.2399	55.3237

21	5	175.79	96.06	167.30	190.91	212.18	76.25	1.2426	52.7470
21	6	171.96	74.23	176.93	231.59	220.18	73.26	1.2419	55.0956
21	7	154.23	93.65	168.94	200.75	219.03	74.22	1.2534	49.9237
21	8	147.96	98.92	165.69	191.16	213.61	74.04	1.2537	47.6077
21	9	150.56	72.76	174.35	211.92	215.76	77.67	1.2547	48.3241
21	10	167.57	74.84	173.74	229.93	217.67	74.61	1.2434	52.5519
21	11	160.65	89.66	165.80	215.41	212.80	76.14	1.2498	49.4496
21	12	170.99	77.35	168.21	219.87	214.92	71.32	1.2432	52.1684
21	13	177.00	72.60	173.69	231.08	216.60	74.95	1.2408	54.6109
21	14	175.38	75.24	178.59	193.91	215.84	78.05	1.2394	54.3830
21	15	179.04	90.20	173.17	190.95	212.69	76.03	1.2397	54.2395
21	16	176.85	81.84	182.03	216.11	213.33	76.57	1.2386	54.6805
21	17	158.55	86.44	169.50	231.39	219.78	72.82	1.2504	51.1493
21	18	180.92	69.93	184.03	231.35	224.67	73.51	1.2381	61.7942
21	19	182.44	73.21	184.70	193.45	216.47	78.62	1.2374	57.5723
21	20	173.34	74.67	176.39	236.07	220.91	69.62	1.2418	56.0327
22	1	152.71	89.85	162.89	192.39	212.12	76.02	1.2621	47.7605
22	2	152.73	101.15	161.21	195.24	214.95	74.63	1.2604	48.2742
22	3	157.33	88.00	178.93	227.18	214.83	77.78	1.2482	50.0162
22	4	182.46	73.12	184.69	199.17	217.27	78.88	1.2374	57.8699
22	5	175.94	78.55	173.00	190.23	212.76	77.84	1.2409	53.2144
22	6	173.81	87.10	175.92	206.56	212.94	76.48	1.2410	53.1545
22	7	179.84	74.90	181.38	225.35	216.54	78.14	1.2383	56.3127
22	8	183.25	71.92	184.69	235.06	218.28	79.20	1.2377	58.5406
22	9	146.60	102.08	160.63	190.23	211.17	77.24	1.2728	46.6501
22	10	146.88	92.43	162.13	206.16	213.32	77.83	1.2672	46.8093
22	11	147.00	94.72	164.41	206.67	211.27	77.07	1.2571	47.0061
22	12	151.64	95.15	162.42	216.93	214.08	78.15	1.2574	47.9679
22	13	161.19	98.17	173.62	192.16	215.17	77.13	1.2469	50.5840
22	14	173.87	97.66	171.85	192.38	211.83	77.19	1.2421	52.6849
22	15	146.61	102.37	160.60	190.32	211.28	75.78	1.2731	46.6586
22	16	166.37	101.75	174.37	199.78	215.13	76.06	1.2427	51.9124
22	17	146.60	102.08	160.63	190.73	211.17	77.74	1.2729	46.6485
22	18	146.60	101.58	160.63	190.23	211.17	77.24	1.2729	46.6454
22	19	181.44	72.21	184.20	193.95	215.47	78.87	1.2375	56.7953
22	20	161.15	89.16	165.80	215.91	212.80	76.14	1.2502	49.5282
23	1	163.74	79.69	165.20	200.31	211.65	77.40	1.2501	49.6405
23	2	160.76	77.35	170.34	223.69	216.24	76.87	1.2501	50.2172
23	3	160.17	97.09	180.85	214.90	212.08	77.08	1.2441	50.4820
23	4	182.34	71.45	184.31	216.38	216.76	77.24	1.2377	57.6352
23	5	174.35	84.20	168.69	216.66	217.09	76.15	1.2431	53.6155
23	6	148.75	95.49	163.88	213.54	212.52	77.22	1.2537	47.4388
23	7	179.84	74.90	181.38	225.35	216.54	78.14	1.2383	56.3127
23	8	148.80	89.25	177.93	198.89	212.35	76.55	1.2529	48.0514

74

23	9	162.76	85.91	173.17	213.04	212.13	77.18	1.2462	50.2447
23	10	180.02	73.87	182.95	217.26	217.23	78.63	1.2380	56.7944
23	11	146.60	102.17	160.60	190.74	211.20	77.46	1.2729	46.6486
23	12	164.77	82.94	178.91	201.94	215.24	78.64	1.2421	51.6590
23	13	149.02	92.80	161.73	190.23	212.21	77.24	1.2558	47.1891
23	14	159.60	92.69	165.50	209.70	211.51	76.39	1.2494	49.1544
23	15	168.03	83.46	177.63	222.68	213.55	76.97	1.2421	51.9971
23	16	176.36	78.41	173.84	210.66	215.29	77.73	1.2407	54.0125
23	17	181.95	70.14	183.94	233.31	221.34	73.38	1.2379	59.9247
23	18	176.92	81.59	182.09	216.36	213.33	76.82	1.2386	54.6933
23	19	176.85	81.84	182.03	215.86	213.40	76.75	1.2386	54.6891
23	20	183.25	71.92	184.69	235.06	218.53	79.38	1.2377	58.6438
24	1	159.60	92.69	165.50	209.70	211.51	76.39	1.2494	49.1544
24	2	182.11	72.73	184.64	200.72	219.52	73.98	1.2376	59.0622
24	3	178.63	76.05	177.17	192.14	215.50	78.15	1.2389	55.0749
24	4	160.27	90.39	165.57	211.35	211.54	76.32	1.2497	49.2493
24	5	159.29	83.15	175.25	192.66	215.85	78.48	1.2479	50.2300
24	6	148.90	89.47	161.18	190.23	211.67	77.38	1.2579	47.0115
24	7	166.93	86.74	167.13	195.05	212.68	77.33	1.2458	50.6504
24	8	171.87	82.28	177.98	216.19	215.99	78.17	1.2415	53.4761
24	9	176.77	81.14	180.52	226.20	217.71	78.80	1.2391	55.6978
24	10	178.02	75.19	178.77	201.37	217.23	77.02	1.2387	55.7082
24	11	159.60	92.69	165.50	209.70	211.51	76.39	1.2494	49.1544
24	12	156.40	93.96	164.34	202.80	211.28	76.44	1.2547	48.4038
24	13	182.44	73.21	184.70	193.45	216.47	78.62	1.2374	57.5723
24	14	149.93	98.41	165.32	200.58	211.22	76.50	1.2584	47.6335
24	15	175.08	79.08	169.95	195.99	216.85	76.51	1.2422	53.7344
24	16	169.39	85.53	171.86	190.23	212.04	77.69	1.2426	51.5390
24	17	146.73	102.18	160.66	190.73	211.19	77.74	1.2719	46.6747
24	18	148.80	89.25	177.93	198.77	212.35	76.55	1.2529	48.0511
24	19	168.03	83.46	177.63	222.73	213.42	77.06	1.2422	51.9724
24	20	146.60	101.58	160.69	190.35	211.17	77.24	1.2726	46.6494
25	1	167.60	86.76	177.54	206.64	216.35	76.69	1.2425	52.5759
25	2	146.60	102.09	160.61	190.73	211.19	77.73	1.2729	46.6507
25	3	168.65	81.93	175.45	191.98	213.99	78.52	1.2421	51.9539
25	4	170.89	89.26	172.58	191.16	214.87	77.69	1.2424	52.5078
25	5	156.07	81.48	165.63	190.61	211.84	77.77	1.2532	48.2873
25	6	169.96	85.11	184.28	194.22	215.47	77.94	1.2399	53.5271
25	7	146.60	102.08	160.63	190.73	211.17	77.74	1.2729	46.6485
25	8	163.61	92.08	172.53	211.52	211.34	77.07	1.2456	50.3748
25	9	148.90	89.47	161.18	190.23	211.67	77.38	1.2579	47.0115
25	10	172.61	73.17	181.58	201.72	217.10	75.00	1.2398	54.4357
25	11	167.43	89.27	172.72	206.72	212.83	77.41	1.2429	51.3620
25	12	169.69	82.74	164.27	214.41	214.71	77.55	1.2453	51.3179

25	13	176.39	81.32	178.01	201.45	212.99	77.78	1.2394	53.9806
25	14	168.96	83.80	176.68	208.24	212.11	77.38	1.2423	51.8856
25	15	163.98	99.31	164.65	222.75	219.12	70.89	1.2519	51.9088
25	16	179.42	85.59	178.11	198.35	218.30	75.14	1.2387	56.7232
25	17	182.71	73.37	184.82	199.17	217.27	79.07	1.2374	57.9721
25	18	175.94	78.55	173.00	190.23	212.76	77.59	1.2409	53.2197
25	19	148.90	89.59	161.18	190.48	211.80	77.63	1.2579	47.0132
25	20	164.77	83.12	178.97	202.00	215.49	78.89	1.2420	51.7123

Bibliography

[1] Ernesto Benini, Professore associato confermato, Università degli Studi di Padova.
Propulsione Aerea.
2005 Cleup SC, "Coop. Libraria Editrice Università di Padova", via G. Belzoni 118/3 - Padova

[2] J. Seddon, E.L. Goldsmith,
Intake Aerodynamics.
American Institute of Aeronautics and Astrinautics, Inc.
Educational Series, 1999.

[3] Richard J. Re and William K. Abeyounis.
A Complete Investigation of Three NACA 1-Series Inlets at Mach Numbers up to 0.92.
Langley Research Center, Hampton, Virginia, 1996

[4] John D. Anderson, Jr.
Fundamentals of Aerodynamics, Fifth Edition.
McGraw-Hill, 1221 Avenue of the Americas, New York, NY 10020, 2011

[5] Pointwise Y+ Calculator
https://www.pointwise.com/yplus/

[6] Frank M. White, University of Rhode Island.
Fluid Mechanics, Seventh Edition.
McGraw-Hill, 1221 Avenue of the Americas, New York, NY 10020, 2011

[7] Ansys Inc User Guide.
2018 SAS IP, Inc.

[8] MATLAB User Guide.
https://it.mathworks.com/help/matlab/

[9] Ascher H. Shapiro, Professor of Mechanical Engineering, Massachusetts Institute of Technology.
The Dynamics and Thermodynamics of Compressible Fluid Flow.
John Wiley and Sons, Inc, 1953

[10] Kwang-Yong Kim, Abdus Samad, Ernesto Benini.
Design Optimization of Fluid Machinery: Applying Computational Fluid Dynamics and Numerical Optimization.
John Wiley and Sons Singapore Pte. Ltd, 2019

[11] Dr. Thomas Sederberg.
BYU Bézier curves.
https://web.archive.org/web/20060221000535/http://www.tsplines.com/resources/class_notes/Bezier_curves.pdf